Physics Faculty

Physics Department

Trabajo de Fin de Grado

Femtosecond laser nanofabrication of subwavelength diffractive structures: fabrication and experimental characterization

---

Author: Nereida Ponzoa González

Academic tutor: Dr. Airán Ródenas Seguí

2022 - 2023

Resumen

En el presente trabajo se van a fabricar redes de difracción mediante un método relativamente reciente llamado nanolitografia 3D. Este consiste en, mediante un láser de femtosegundos, grabar sobre un cristal la estructura que queramos. Después este cristal será sometido a ataque químico, dejando poros en el cristal en forma de la estructura previamente grabada. En nuestro caso, al tratarse se una red de difracción, grabaremos líneas horizontales en el cristal. Queremos lograr obtener una red de difracción cuya eficiencia en el primer orden de difracción sea casi del 100%, para ello nos basaremos en distintos trabajos ya realizados para elegir los parámetros de fabricación. Se han hecho un total de dos redes de difracción, ambas con parámetro de red $\Lambda = 0.0005mm$ y con una tasa de repetición de 1MHz (pulsos por segundo). En la primera de ellas su velocidad de escaneo ha sido de 10 $\frac{mm}{s}$, se ha realizado sobrescritura y se han utilizado 5 potencias: 22, 19, 16, 13 y 10 mW. Para la segunda de las fabricaciones se utilizó una velocidad de escaneo de $1\frac{mm}{s}$ y se seleccionaron 6 potencias: 22, 20, 18, 16, 14 y 12 mW. La primera de las fabricaciones no salió como se esperaba por dos motivos, en primer lugar solo se grabaron fragmentos de 3 de las 5 potencias y en segundo lugar se generaron muchos nanocracks durante el grabado; por estos motivos no se pudieron extraer muchos resultados.

El primero de los resultados que hemos podido observar es un cambio anisótropo al grabar la red, pues solo transmite luz polarizada verticalmente. También hemos visto que para las potencias más altas el cristal se empieza atacando con más velocidad, pero que estas acaban llegando a la saturación de modificación mucho antes que las potencias menores. Hemos ajustado los datos de la segunda de las fabricaciones a una función de difusión, obteniendo que tipo de difusión sigue el ataque químico dentro de los poros en función de la potencia. Hemos concluido que al principio todas las potencias siguen una difusión Browniana, y que después las potencias más intensas pasan a tener una difusión subdifusiva y las menos intensas una superdifusiva. Para finalizar, se mencionan algunas de las mejoras que se pueden realizar en los experimentos y algunos proyectos que se quieren realizar en un futuro.

Palabras clave: Nanolitografía 3D, Red de Difracción Sublongitud de Onda, Ataque Químico, Distribución de difusividad

Abstrat

In the present work, diffraction gratings will be fabricated using a relatively recent method called 3D nanolithography. This consists of, by means of a femtosecond laser, engraving on a crystal the structure we want. This crystal is then subjected to a wet chemical etch leaving pores in the crystal in the form of the previously engraved structure. In our case, being a diffraction grating, we will engrave horizontal lines on the crystal. We want to obtain a diffraction grating whose efficiency in the first order of diffraction is almost 100%, for this we will be based on various works already done to choose the manufacturing parameters. A total of two diffraction gratings have been made, both with grating parameter $\Lambda = 0.0005mm$ and with a repetition rate of 1MHz (pulses per second). In the first one its scan speed has been 10 $\frac{mm}{s}$, overwriting has been performed and 5 powers have been used: 22, 19, 16, 13 and 10 mW. For the second of the fabrications, a scan rate of $1\frac{mm}{s}$ was used and 6 powers were selected: 22, 20, 18, 16, 14 and 12 mW. The first of the fabrications did not come out as expected for two reasons, firstly only fragments from 3 of the 5 powers were etched and secondly many nanocracks were generated during engraving; for these reasons not many results could be extracted.

The first of the results that we have been able to observe is an anisotropic shift when the lattice is engraved, as it only transmits vertically polarized light. We have also seen that for the higher powers the crystal starts attacking faster, but that these end up reaching modification saturation much earlier than the lower powers. We have fitted the data from the second of the fabrications to a diffusion function, obtaining which type of diffusion follows the chemical attack inside the pores as a function of power. We have concluded that at the beginning all the powers follow a Brownian diffusion, and afterwards the more intense powers become subdiffusive and the less intense ones a superdiffusive diffusion. Finally, we mention some of the improvements that can be made in the experiments and some projects that we want to carry out in the future.

Keywords: 3D Nanolitography, Diffraction Grating Wavelength Sublength, Chemical Attack, Diffusivity Distribution

Contents

1 Introduction **1**
1.1 Motivation and applications . . . 1
1.2 Objectives of the project . . . 2

2 Theoretical Framework **3**
2.1 Introduction to diffraction . . . 3
2.1.1 Huygens' Principle . . . 4
2.1.2 Interferences . . . 4
2.2 Diffraction gratings . . . 5
2.3 Diffusivity . . . 8

3 Methodology **9**
3.1 Setup of the first harmonic . . . 9
3.2 Construction of the second harmonic setup . . . 11
3.2.1 Materials . . . 11
3.2.2 Scheme . . . 12
3.3 Fabrication of a diffraction grating . . . 13
3.3.1 Laser alignment . . . 13
3.3.2 Glue the sample with enamel . . . 13
3.3.3 Place the sample on the platform and center it . . . 14
3.3.4 Immerse the sample in reversing oil . . . 14
3.3.5 Focus . . . 14
3.3.6 Calibration of the sample platform . . . 14
3.3.7 Engraved . . . 15
3.3.8 Polishing . . . 16
3.3.9 Chemical attack on the diffraction grating . . . 17
3.4 Manufacturing . . . 18
3.4.1 Work results . . . 18
3.4.2 First manufacture . . . 20
3.4.3 Second manufacture . . . 21
3.4.4 Diffraction angle measurement experiment . . . 22

4 Analysis and discussion of results **23**
4.1 First manufacture . . . 23
4.1.1 Observation under the optical microscope before starting to attack . . . 23
4.1.2 First Etch . . . 25
4.1.3 Second Etch . . . 25
4.1.4 Third Etch . . . 26

4.1.5 Fourth Etch . . . 27
4.1.6 Fifth Etch . . . 27
4.2 Second manufacture . . . 28
4.2.1 First Etch . . . 28
4.2.2 Second Etch . . . 29
4.2.3 Third Etch . . . 29
4.2.4 Fourth Etch . . . 30
4.2.5 Sample profile images . . . 31
4.3 Results . . . 31

5 Conclusions and improvement projects 37

6 Bibliography 39

7 Annex 40
7.1 Annex 1: First manufacture code . . . 40
7.2 Annex 2: Second manufacture code . . . 42

1 Introduction

Esta sección comienza explicando los orígenes de las redes de difracción, descubiertas primero en la naturaleza y diseñadas después por el hombre. También se discuten los tipos de rejillas que existen en la actualidad y algunas de las formas en que se clasifican. Se mencionan algunos de los métodos utilizados para crearlas, así como algunos de los muchos usos de las redes de difracción en la actualidad. También se mencionan los objetivos que queremos alcanzar durante este trabajo.

1.1 Motivation and applications

The first diffraction grating was created in 1673 by James Gregory, at that time, it was already known about the colors that compose white light because the gratings were built a few years after Isaac Newton's experiment with prisms. The first diffraction gratings were things that we can find in nature such as bird feathers, butterfly wings or some precious stones. The first man-made diffraction grating was built in about 1785 by David Rittenhouse who inserted hairs between 2 firmly screwed screws. From that time until now, gratings have been evolving little by little thanks to new technologies and manufacturing processes and will continue to do so in the coming decades. To put it simply, a diffraction grating consists of a periodic structure that is capable of diffracting light in different orders, both in transmission and reflection. In the section 2.2 we will discuss in more depth how these curious structures work.

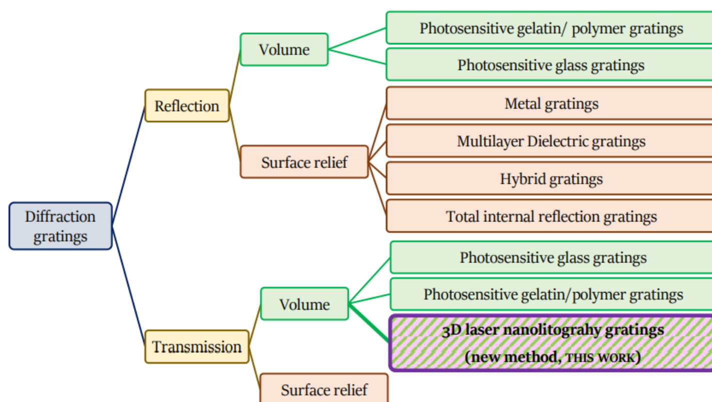

Figure 1: Classification of different diffraction grating [1]

As can be seen in the Figure 1, a great diversity of techniques for making diffraction gratings have been developed over time. Nowadays, gratings can be classified according to their principle of operation (whether they diffract light in transmission or in reflection), according to the material of which the grating is composed and according to the lithography technique used. We should also not forget that there are gratings that are created inside the material, these will be the volume gratings; and gratings that are created on the surface, these will be the surface gratings. For this project, highlighted in purple in the image, we will focus on making diffraction gratings using an innovative method called 3D laser nanolithography gratings. This technique consists of writing your grating using a femtosecond laser inside a crystal (for this project we will use Yttrium Aliminium Garnet, which we will refer to as YAG), therefore we will obtain a diffraction grating in the volume. In particular

we will focus on creating subwavelength gratings, as these under certain conditions will be able to transmit almost all the received intensity to the first order of diffraction, as we will see below.

Diffraction gratings are used in many fields of physics. They are necessary in spectroscopy, to acquire the spectra of a sample or a star, and they can also be used to make optical filters as well as to amplify the intensity of ultra-short pulses of lasers, among many other applications.

In summary, it is essential to find new ways of making diffraction gratings, which should be very durable and with high resolution.

1.2 Objectives of the project

The main objectives of this project are to expand the knowledge acquired in the course on diffraction gratings, to build the second harmonic setup and to build gratings using the innovative technique of 3D laser nanolitography gratings. Then, the diffraction gratings will be studied to see if they are in agreement with the simulations made by Alfredo Casanovas Melián in his TFM [1]. Finally, we want to study what happens inside the nanopores during chemical wet etch, so we will fit the data obtained to a diffusion function and see what kind of diffusions occur.

2 Theoretical Framework

En esta sección se van a introducir los fundamentos teóricos necesarios para poder entender el trabajo a leer. En primer lugar, se empieza hablando sobre el experimento que realizó Grimaldi el cual fue uno de los primeros en poder apreciar el fenómeno de la difracción. Después introduciremos el principio de Hyudens el cual nos permite predecir la forma geométrica que tendrá un frente de ondas con el tiempo. En tercer lugar, hablaremos sobre las interferencias, uno de los fenómenos claves para entender el funcionamiento de una red de difracción. En cuarto lugar, hablaremos, por fin, del fundamento físico detrás de una red de difracción, el cual consiste en que cuando un haz de luz incide sobre una estructura periódica de rendijas se crean frentes de onda en ellas, estas nuevas ondas producirán interferencias y crearán un patrón. Podremos ver que se crearán órdenes de difracción tanto en reflexión como en transmisión y que estos van a depender tanto de la estructura de la red, como de la longitud de onda que tenga nuestra onda incidente. Después veremos que hay distintos tipos de redes de difracción en función de como sea su parámetro de red, y estas son las redes de órdenes altos, las de órdenes bajos, las sublongitud de onda (con órdenes de difracción) y las sublongitud de onda (con solo el orden m= 0). Luego se hablará sobre el ángulo de Littrow, el cual es un ángulo donde se puede hacer máxima la difracción para un orden en concreto. En último lugar, dado que las redes de difracción se fabrican mediante ataque químico, el cual produce la difusión de un ácido dentro del cristal en las zonas irradiadas, se han ajustado los datos a un proceso de difusión. Por tanto, se hablará del movimiento browniano, así como de las distintas distribuciones que encontramos en función del coeficiente α las cuales serán superdifusiva ($\alpha > 1$), normal o Browniana ($\alpha = 1$) y subdifusiva ($\alpha < 1$).

2.1 Introduction to diffraction

Before explaining what a subwavelength diffraction grating is, I would like to give a brief introduction to how a diffraction grating works.

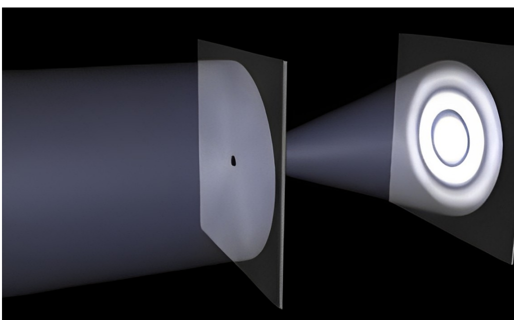

Figure 2: Grimaldi's experiment [2]

Diffraction is the distortion or variation in the direction of wave propagation when it encounters an obstacle that has dimensions comparable to its wavelength. This phenomenon not only occurs in diffraction gratings but also in nature, where it can be found in events such as rainbows, halos around point sources of light, such as around the Sun or the Moon, and bird feathers. As told in [2] Grimaldi in 1648 made an experiment where he made sunlight pass through a perforation made in a cardboard. In this experiment he not only noticed that the beam of light became larger but also that lighter and darker stripes were created (actually colored because he did it with a white light source). This phenomenon could not be explained until Fresnell related it to the wave

theory. This is a very simple experiment but it allows us to see the phenomenon of diffraction in a very simple way.

Before explaining in depth what a diffraction grating is, it is essential to explain Huygens' principle.

2.1.1 Huygens' Principle

The Huygens principle provides us with a geometrical model to predict how a wave front of a known wave will move. It assumes that each point of a primary wave front produces an emitting focus of spherical secondary waves that have the same frequency as the previous ones. These propagate in all directions and with the same velocity as the primary wave for each of the points.

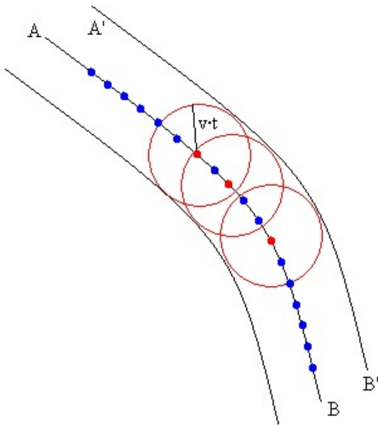

Figure 3: Huygens' Principle [3]

Now suppose that we want to calculate the new wave front of the line AB shown in 3 when a time t has elapsed, and supposing that the waves propagate at a velocity v. The first thing we have to do is to place different focuses of emission of waves (the blue and red dots), from these points we will suppose that a circular wave propagates. Then, to represent this circular wave we will draw a circle with radius v·t, because this is the distance that the wave has traveled in a time t, taking as center the supposed focus. If we take infinite focuses in the wave front AB we will obtain a new wave front A'B' shown in the Figure 3.

Now suppose that we pass a beam of monochromatic light (with a single wavelength) through a hole that has a size less than or equal to its wavelength. The light will propagate until it hits the slit, in this slit the light will only be able to create an emitting focus in the hole of the slit, therefore the light will change direction forming what is known as diffraction.

A focus is a point emitting plane waves in all directions and the geometric figure formed by joining all the points in phase of the emitted waves is known as a wave front.

2.1.2 Interferences

When two waves collide with each other, what is known as interference is produced, this phenomenon consists in the addition of the waves algebraically. We will say that a constructive interference has occurred when the waves are in phase and therefore their amplitude increases. We will say that two waves are in completely destructive interference when the waves are in opposite phases, i.e. when the amplitude of one increases, the other decreases. We will say that the waves are partially destructive interference if the waves are not in phase.

2.2 Diffraction gratings

Once we know what diffraction is and how it is generated, we can talk about what a diffraction grating is.

A diffraction grating is a periodic structure formed by a series of grooves placed side by side, it is periodic because all of them are separated by a fixed distance d. To explain well the functioning of a diffraction grating, we will use the Figure 4 extracted from [4]. As we know, a wave front is a geometric figure that joins all the points that are in phase of the different waves, so in the image we find wave fronts of minima (in blue) and wave fronts of maxima (in red). Now suppose that we emit a beam of monochromatic light towards two slits at a distance d from each other, whose size is less than or equal to the wavelength of the incident wave. As we know, by the Hyugens principle, two wave emitting focuses will be created in the center of the two slits. These waves created by the two new focuses will interfere with each other creating constructive interference (at the points where two red lines cross), completely destructive (when the red and blue lines cross) and partially destructive (at the rest of the intermediate points). If at a certain distance we put a detection screen we will be able to see the interference pattern, which is based on different peaks of maximum intensity which will be known as diffraction orders.

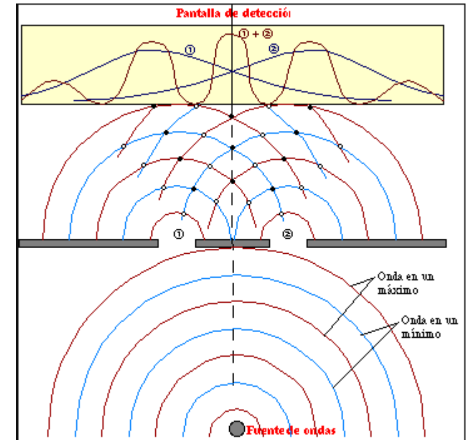

Figure 4: Diagram of a diffraction grating [4]

As we have seen in the introduction there are basically two types of diffraction gratings: transmission and reflection gratings. As the name indicates, transmission diffraction gratings diffract when light is transmitted and reflection diffraction gratings diffract when light is reflected.

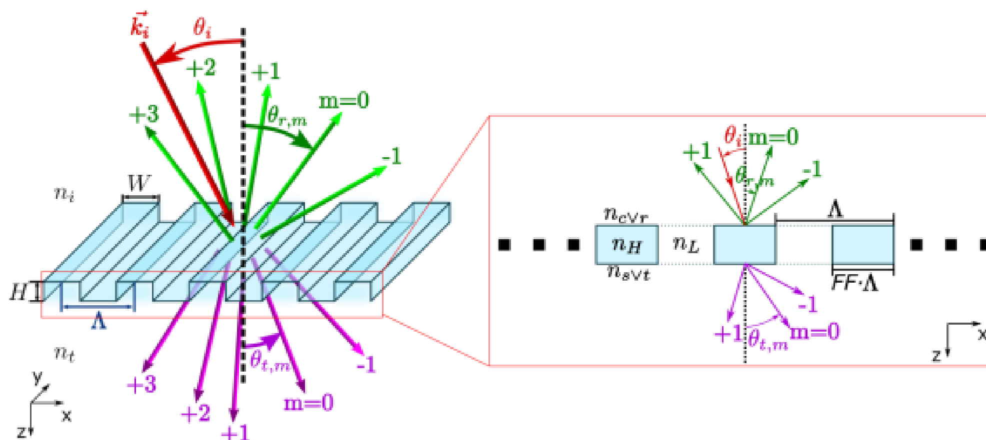

Figure 5: Schematic diffraction grating [1]

In Figure 5 we can see on the left a scheme of how light diffracts as well as the parameters of a

diffraction grating, and on the right we can see the transversal plane of the grating schematized indicating refractive indexes.

In the image on the left we can see how a plane wave, with wave vector $\overrightarrow{k}_i$ (in red), is incident on a diffraction grating, diffracting as a sum of plane waves in different orders of refraction expressed as m. In these diffracted waves we will have those that are transmitted (with wave vector $\overrightarrow{k}_t$ in purple) and those that are reflected (with wave vector $\overrightarrow{k}_r$ in green). The angle at which our plane wave is incident is expressed as θ_i, and the angles at which the different orders exit show as $\theta_{r,m}$ for those reflected, and $\theta_{t,m}$ for those transmitted. We will call the grating period or "pitch" the Λ parameter which later will be of vital importance. The lattice height is assigned the letter H and the thickness is assigned the letter W. Diffraction orders can be predicted using the equations 1 for transmission and 2 for reflection.

$$n_r \cdot sin(\theta_{r,m}) = n_i \cdot sin(\theta_i) + m\frac{\lambda_0}{\Lambda} \quad (1)$$

$$n_t \cdot sin(\theta_{t,m}) = n_i \cdot sin(\theta_i) + m\frac{\lambda_0}{\Lambda} \quad (2)$$

These equations can be used for any diffraction grating, although they cannot predict things like the intensity of each order or the polarization.

If we now focus on the image on the right of the Figure 5 we can see that a diffraction grating is basically composed of four refractive indices. We will have a material with a high refractive index, n_H; a material with a low refractive index, n_L, then we will have the materials surrounding the lattice in which we will have the cover n_C and the substrate n_S. In our case $n_L = n_C = n_S = n_{YAG}$ and $n_H = 1$ because the diffraction grating is composed of air pores inside the YAG crystal.

We will define the diffraction lattice filling factor (FF) as $FF = \frac{l}{\Lambda}$ where l will be the pore width and Λ the lattice constant, i.e. how far apart the pores are engraved.

We can relate the refractive indexes shown in the equations 2 and 1 and 5 using the equalities: $n_i = n_r = n_C$ and $n_t = n_S$.

As mentioned before, choosing the Λ value is fundamental when constructing diffraction gratings, because when this parameter decreases, so will the diffraction orders in both transmission and reflection. In the equation 3 we see defined the diffraction index for a diffraction grating, this index can only be used in subwavelength diffraction gratings, where Λ is smaller than the wavelength.

$$n_{avg} = \sqrt{n_H^2 \cdot FF + n_L^2 \cdot (1 - FF)} \quad (3)$$

According to our reference [1] we can predict the diffraction order at which a lattice will arrive

using the equations 3, 2 and 1 and imposing the condition $|sin(\theta_m)| > 1$. Consequently we can distinguish four types of behaviors in the diffraction gratings, which can be seen represented in Figure 6.

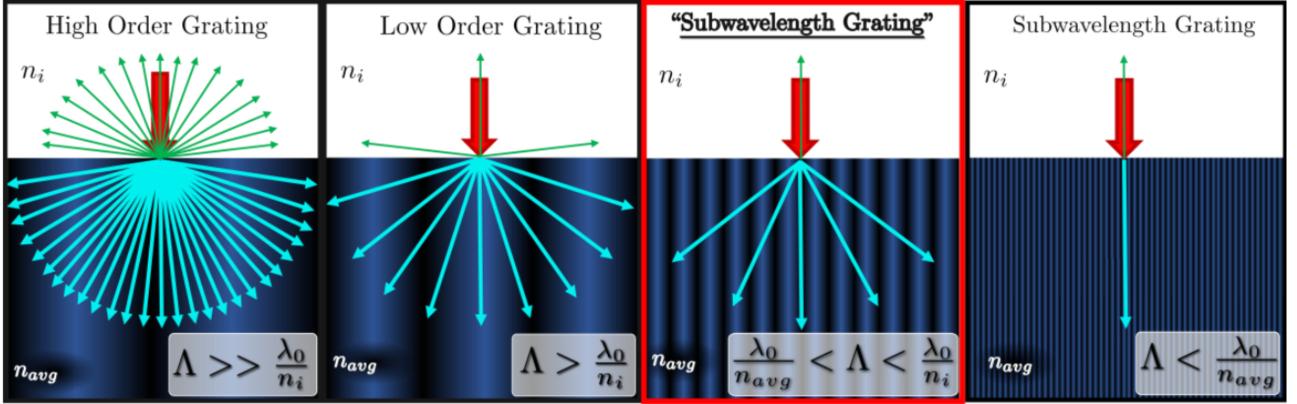

Figure 6: Types of diffraction gratings. The one studied in this TFG is highlighted in red (considering $n_{avg} > n_i$) [1]

Where λ_0 is the wavelength of the incident wave in vacuum.

In Figure 6 we can see that if the $\Lambda >> \frac{\lambda_0}{n_i}$ then we will have a large number of diffraction orders in both reflection and transmission obtaining a "High Order Grating". Reducing a little the difference between both coefficients we will obtain what is known as "Low Order Grating". When $\frac{\lambda_0}{n_{avg}} < \Lambda < \frac{\lambda_0}{n_i}$ we will have a subwavelength grating. In this case the grating can be designed to have no reflection and have a single diffraction order. If $\Lambda < \frac{\lambda_0}{n_{avg}}$ then only 0th order propagates, so no light is diffracted.

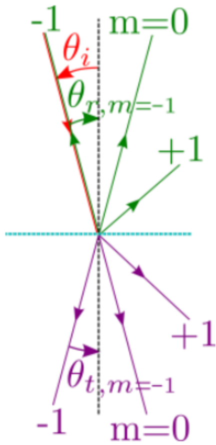

Figure 7: Diffraction grating under Littrow configuration [1]

We will say that the transmission for an order m is maximum when the system is working under the Littrow configuration or Littrow mounting. This configuration will happen when we have $\theta_{Litt} = \theta_i = -\theta_{r,m}$, in the equation 4 we see how the Littrow angle can be calculated.

$$\theta_{Litt} = asin(-m\frac{\lambda_0}{2 \cdot \Lambda \cdot n_i}) \tag{4}$$

Where n_i is the refractive index of the incident medium, $lambda_0$ is the incident wavelength, Λ is the lattice constant and m is the diffraction order. We are particularly interested in the order m= -1, so looking at the Figure 7 we obtain the relations $\theta_i = -\theta_{r,-1} = -\theta_{t,-1}$.

Since diffraction gratings are fabricated by chemical etching, which produces the diffusion of an acid inside the crystal in the irradiated areas, the data have been fitted to a diffusion process. It is therefore of vital importance to introduce the concept of diffusivity.

2.3 Diffusivity

Brownian motion, discovered by the Scotsman Robert Brown, is the random motion observed in particles in a fluid medium as a result of collisions with the molecules of the fluid. Einstein in one of his works formulated the diffusion equation of Brownian particles, which relates the mean square displacement of a Brownian particle with its diffusivity constant and time. Obtaining the equation $D = \lim_{t\to\infty} \frac{<x^2(t)>}{2\cdot t}$

The diffusion process occurs when a group of particles move from a region of high concentration to an area of low concentration until a uniform distribution is obtained. These are subject to Fick's laws. Diffusion is often described by a power law that takes the form of the equation 5.

$$x^2 = 2 \cdot D \cdot t^{\alpha} \tag{5}$$

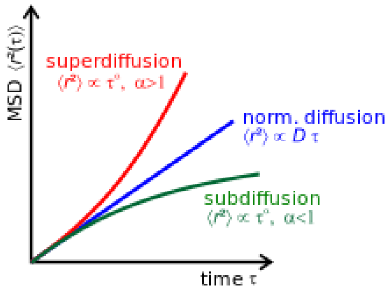

Figure 8: Variance versus time

We will find a normal or Brownian diffusion when $\alpha = 1$, this indicates that this process will be governed by a Gaussian probability density function whose variance will grow linearly with time. We can also find that the process does not have a linear relationship with time, these types of processes are known as anomalous diffusivity. We can find two types of anomalous diffusivities, when $\alpha > 1$ we will have a superdiffusive process and when $\alpha < 1$ a subdiffusive one. In Figure 8 we can see a representation of the three types of diffusivities.

3 Methodology

En esta sección se va a explicar un poco cuál es la metodología utilizada en este trabajo. Se va a empezar explicando el setup del primer armónico que ya está montado en el laboratorio. Este setup, el cual se aprecia en la Figura 9 fue en el que nos basamos para construir el setup del segundo armónico, el cual se aprecia en la Figura 12. Una vez ya explicados los distintos setups pasamos a explicar el proceso que se lleva a cabo para obtener nuestra red de difracción. Estos pasos consisten en alinear el láser, pegar la muestra con esmalte, centrar la muestra, poner el aceite de inversión, enfocar, calibrar la plataforma, escribir con el láser, pulir y por último atacar. Después se explicarán las potencias con las que vamos a grabar en nuestras redes de difracción y porque. Básicamente en [1] se realizan unas simulaciones donde se optimiza la longitud y anchura que deben tener nuestros poros para tener una buena eficiencia de difracción para el primer orden. Elegiremos un rango de esa simulación y buscaremos en [5] y [6] que potencias debemos utilizar para hacer poros de ese tamaño. Después de explicar distintos conceptos se explicarán los parámetros de fabricación utilizados para las dos fabricaciones realizadas. Por último hablaremos sobre el experimento que se quiere realizar una vez fabricadas las redes, el cual nos permitirá saber si hemos realizado las redes de difracción acorde a las simulaciones.

3.1 Setup of the first harmonic

The laser we have in the laboratory can emit for two different wavelengths, depending on the harmonic. For the first harmonic it emits radiation with a wavelength in the infrared range, and for the second harmonic it emits in the green range. Before starting with the construction of the setup of the second harmonic, which is one of our main objectives, we must understand the setup performed in the infrared range.

In Figure 9 we can see a simplified schematic of the infrared laser setup.

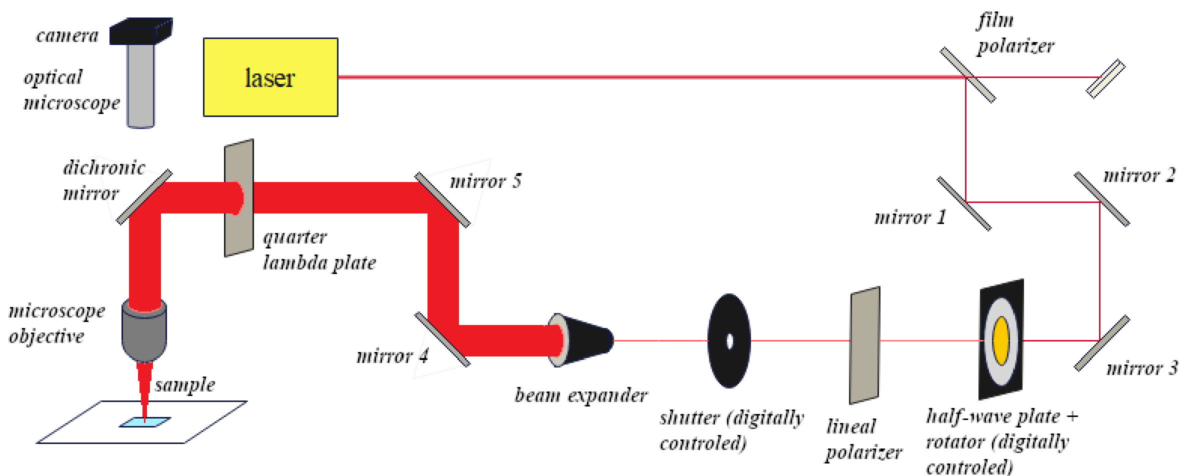

Figure 9: Setup of the first harmonic

To understand how the setup for the first harmonic works, we will follow the trajectory of the light and we will explain the changes it undergoes. We start at the laser, which is the point from where the light comes out. At this point the light comes out with vertical linear polarization and with a wavelength of 1030 nm. Then the light beam meets a polarizer film, which reflects only 20% of the light that initially arrives and the rest is transmitted. Then we find three dielectric mirrors which are responsible for reflecting the light to the half-wave plate, it is important to have a good number of mirrors to guide the light so the number of degrees of freedom increases allowing us to align the laser more easily. The half-wave plate is placed inside a digitized rotor, which allows us to control how much the plate is rotated with respect to the vertical. We know that as it passes through the half-wave plate the polarization will still be linear but it will acquire the same inclination as we have set the plate. Then we will find a linear polarizer placed vertically, so that it will only let pass a part of the beam that reaches it, since the polarization will arrive diagonally due to the average lambda sheet. So, if we call P to the initial power that reaches the laser, and the beam arrives with a lineal polarization rotated at an angle of α with respect to the vertical, the linear polarizer will only let pass a power $P \cdot cos(\alpha)$. Thus we can control the power with which we write on the crystal by simply rotating the angle of the middle lambda plate. Then we can find a shutter which can be controlled digitally, it allows us to let the light beam pass or not. Then we find a beam expander, which as its name suggests is responsible for expanding the beam, followed by two dielectric mirrors to guide the beam. Then we will find a lambda-quarter plate that will be in charge of passing the polarization from linear to circular. Then we see a dichronic mirror which reflects light in one direction and transmits it in the other. All these elements are optimized for the infrared range, for example the mirrors will be dielectric being half invisible to visible light but reflecting almost 100% of the incident light in the infrared. Then we find a microscope objective, this will allow us to focus the laser inside the sample. To focus it, the camera attached to the optical microscope will be used. It should be noted that the platform where the sample is placed is completely digitized and can be moved by the computer in the three axes (x, y and z).

In Figure 10 we can see part of the setup of the first harmonic assembled in the laboratory.

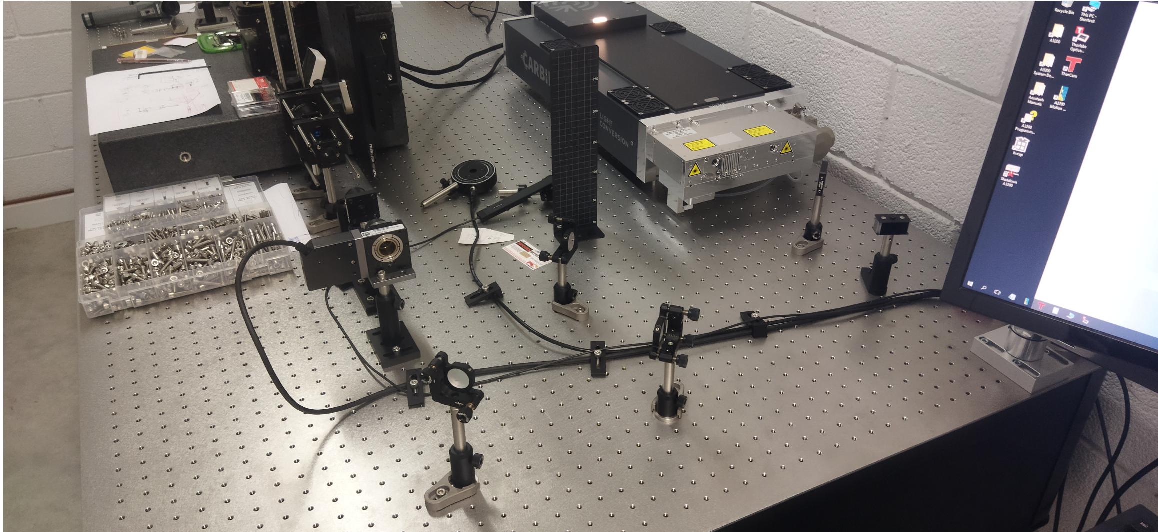

Figure 10: Setup of the first harmonic (infrared)

3.2 Construction of the second harmonic setup

Once the elements contained in the infrared setup and their operation are known, it is time to build the second harmonic setup. The theoretical basics will be more or less the same as for the first setup, with the difference that the elements will now be optimized for the 515 nm range, which is the wavelength of the second harmonic. In the Section 3.2.1 we will go into more detail on the materials that have been purchased.

3.2.1 Materials

In Figure 11 we can see all the materials that will be used to assemble this setup.

Figure 11: Materials used to assemble the green laser setup.

1. **Supports** Mounts are used to place optical objects in place. These have a magnetized base to make it more difficult to move them accidentally once they are in place, but they can be moved with some ease.

2. **Mounts** The mounts are used to hold the optical elements, specifically we will use them to place the dielectric mirrors. These mounts are placed on top of the brackets by means of a thread.

3. **Polarizer Support** Once the linear polarizer is placed inside the mount, we will proceed to screw it with the support.

4. **Screws** The screws are used to place the different optical elements in the mounts.

5. **Mobile mount** One of the dielectric mirrors will be placed on this mount. The particularity of this mirror is that it can be moved to one side allowing to change the optical axis on which it is working.

6. **Polarizer Mount** The lineal polarizer is placed inside this mount.

7. **Dielectric mirrors** These dielectric mirrors reflect from 400 to 750 nm so they will perfectly reflect the 515 nm second harmonic.

8. **Fasteners** These are used so that once the position of the optical object has been decided, it can be fixed to the work table and can no longer move.

9. **Clamps** They are placed in the silver part of the brackets and are used to be able to remove some optical element from the black bracket so that the height is saved.

10. **Half-Wave Plate ($\frac{\lambda}{2}$)** As mentioned in section 3.1 it is responsible for rotating the lineal polarization of the laser beam.

11. **Quarter-Wave Plate ($\frac{\lambda}{4}$)** It is responsible for switching from linear to circular polarization.

12. **Back Side Polished** This is a special dielectric mirror that only allows light to be transmitted in one direction and reflects in the other.

13. **Linear Polarizer** It is responsible for allowing only vertically polarized light to pass through.

3.2.2 Scheme

In the following figure we have made a scheme of how we plan to build the second harmonic set up.

As can be seen, the setup of the first harmonic has been interspersed with that of the second harmonic, since we have to continue using the same shutter and beam expander. We can see that it is decided whether to engrave with one or the other a movable mirror located between the middle lambda plate of the first setup and the shutter. The physical basis is exactly the same as explained in the section 3.1 with the exception that now the lambda media plate has to be rotated manually, since no support has been set up to digitize its rotation. Also, as the path is longer, more mirrors have had to be placed to reach the shutter properly.

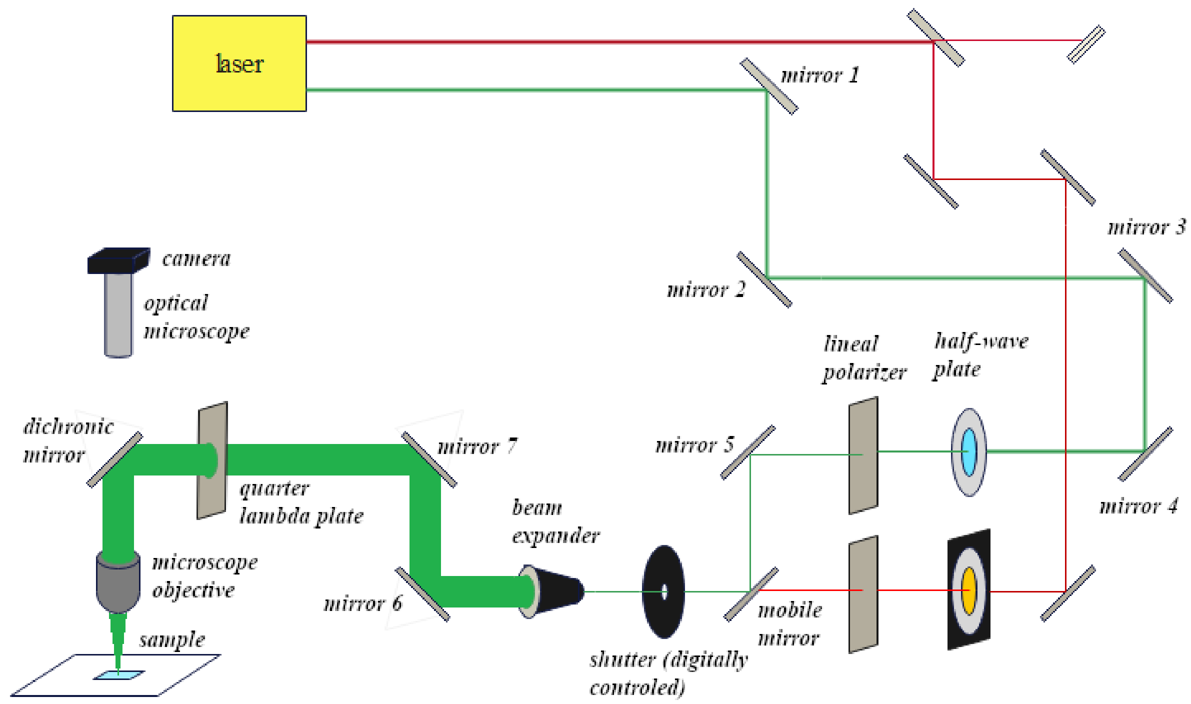

Figure 12: Esquema setup segundo armónico

3.3 Fabrication of a diffraction grating

In this section we will summarize the steps that have been followed to obtain the diffraction grating and the reasons for each of these steps.

3.3.1 Laser alignment

The first thing to do to start manufacturing is to align the laser. To do this, phosphorescent plates with a hole in the center are used.

3.3.2 Glue the sample with enamel

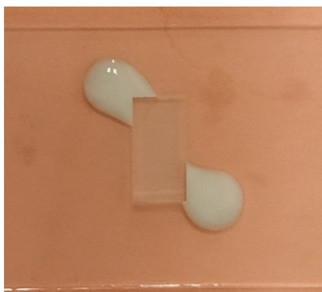

Figure 13: Crystal glued to the slide

In order to be able to manufacture the sample well, it is crucial that it does not move during the writing process. The supports of the platform where the lithography is carried out are the size of a slide, therefore, a much larger size than the size of the samples to work with. As the sample is much smaller than a slide, it is essential to glue the sample with enamel in order to start the fabrication of the diffraction grating. It is only necessary to place two small drops of enamel, one at each end of the crystal to fix the sample. Before proceeding with the rest of the steps, it is very important to wait a few hours until the enamel is completely dry, otherwise we run the risk of the crystal moving while the engraving is being done.

3.3.3 Place the sample on the platform and center it

Once the sample is dry (it is not necessary that it is completely dry, although it is advisable) we will proceed to place the sample on the platform where the fabrication is going to be done. First we will place it leaving the screws used to fix the sample a little loose, so that the sample cannot move by mistake but the position can be modified manually. Once the crystal is placed we will look through the optical microscope to make sure that the sides of the crystal are straight. If they are not, the sample will be moved manually until they are completely aligned. Once the desired position is obtained, the sample is fixed definitively to the platform. This step is very important, because if the crystal is not straight we will start to record the diffraction grating outside the crystal.

3.3.4 Immerse the sample in reversing oil

Our microscope has a very high numerical aperture (NA) of 1.4NA, to achieve this it is crucial to place the immersion oil between the sample and the objective. Without oil, the medium between the objective and the sample is air allowing a maximum numerical aperture of 0.9NA, so for higher NAs it is necessary to place a higher index medium between the sample and the objective, either water or oil can be used. We are looking for the highest possible optical resolution, so we are forced to use the highest NA objective available on the market. At the same time this objective has correction for spherical and chromatic aberration.

3.3.5 Focus

Focusing is one of the simplest steps, but also one of the most time consuming. To focus we must look inside the crystal, then we will move the microscope objective in the z-axis until we see through the camera on top of the microscope, a focused point.

3.3.6 Calibration of the sample platform

To calibrate the platform we will use the camera. We know that, if the focus is well done, when pointing at the sample we will see a sharp point, so it should be sharp at all points of the crystal.

First we will place ourselves on one of the edges of the crystal and define our point x=0, y=0 and z=0. This point will be our origin of coordinates and we will call it O (Figure 14a). Once we have defined our point O in the computer, we will focus the laser as well as we can on our origin. Let's suppose that we first want to level the platform on the x-axis. The first thing we will do is to move a very small distance on that axis, we will call this distance Δx. In the Figure 14b we can see in a schematic way the steps that will be done. Our objective is to find the angle of inclination, which in this case is represented by the Greek letter α. If the platform is tilted when moving laterally over the sample we will see how the laser goes out of focus. Once in the position Δx we are going to move little by little the microscope objective until we see that the laser is focused again. As the microscope objective is digitized we will be able to know how much the vertical axis has moved, therefore we will be able to obtain

the value of Δz. Once we have the two values, we are going to calculate the value of α using the expression $\alpha = arctan(\frac{\Delta z}{\Delta x})$, which we can obtain by observing the Figure 14b. Once the angle is obtained, we only have to multiply it by a coefficient (different if the angle is positive or negative) which will convert our angle into lines that we have to move from some wheels located on the platform. For the x-axis we must move the wheel with the letter H and for the y-axis the wheel with the letter M. Once the lines are moved, we will focus the focus on the ends of the sample and we will repeat the same process but now taking a Δx higher than the previous one. We repeat this until the platform is already leveled. Once the x-axis is level we repeat the same but now taking a Δy.

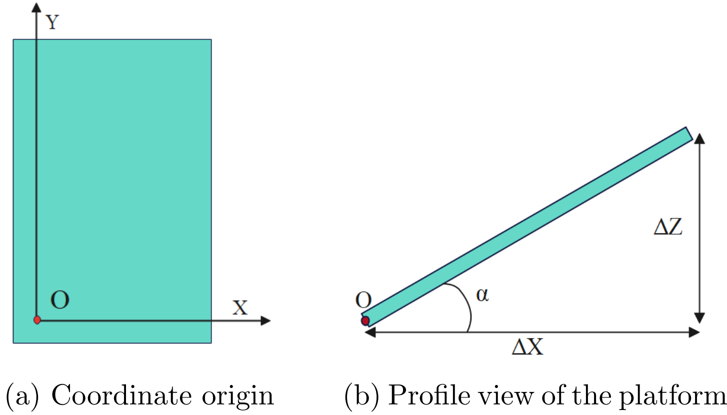

(a) Coordinate origin (b) Profile view of the platform

3.3.7 Engraved

Once the previous steps are done, we can start engraving our diffraction grating to the YAG crystal. To do this, we will make use of a code that will control the laser automatically doing what we want it to do. We will go into a little more detail on how to write the codes for the laser to work, and in the appendix you can find the two codes that we have used to make the two fabrications.

When we do lithography with the femtosecond laser, we produce a deformation in the crystal lattice of the material. To make it clearer, let's look at the Figure 15. In the figure on the left (15a) we can see a 2D schematic of what would be the crystal lattice of our sample (very simplified). When the laser is shone on, the atoms are displaced, leaving something like what we see in the Figure 15b. As can be seen, the red atoms are the ones that have been forced to move because of the laser. This deformation of the crystal lattice will generate stress on the material. If at some point any of the blue links between the black and red atoms breaks (because it has reached the limit of stress it can withstand) we will have what is known as nanocrack. We must imagine the crystal lattice as an elastic structure, so that once the bond is broken, the accumulated stress will be released and the crystal structure will return to its original shape.

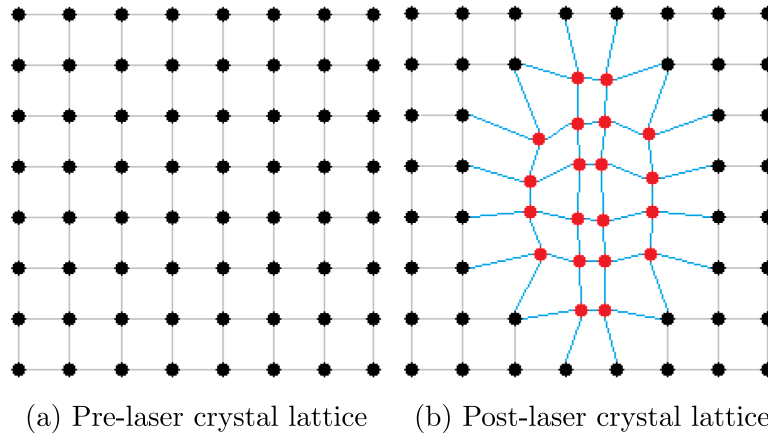

(a) Pre-laser crystal lattice (b) Post-laser crystal lattice

Figure 15: Crystalline lattice before and after laser treatment

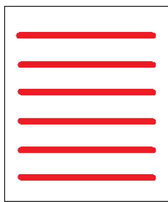

Figure 16

There are certain aspects to be emphasized before moving on to the next step. First of all, the diffraction grating is going to be engraved in the volume and not on the surface. And then, for our diffraction grating, nanotracks will be engraved on the crystal as shown in the Figure 16, i.e. the lines will be engraved horizontally and leaving a certain distance to the edge. The distance between lines and some parameters of the diffraction grating are specific for each of the fabrications, so they will be specified later.

3.3.8 Polishing

Once the diffraction grating has been engraved on the crystal, the sample must be polished. When you engrave a crystal, you do not start engraving it from the end, but you do it a few microns further inward. For the diffraction grating to be visible, it is essential to attack the scratches that have been engraved and we need the solution that will do the attack to enter into the pores. If we did not do this, there would be no way for the attack solution to enter the pores, since the grating is engraved in volume and not on the surface, there would be no way to access it.

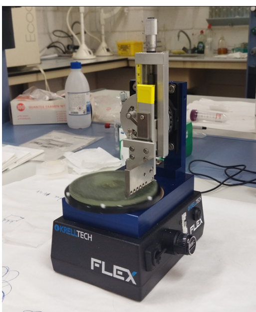

Figure 17: Polishing machine

To perform the polishing, we use an electric polishing machine that we have in the laboratory, which can be seen photographed in the image 17. This device performs its function by rubbing diamond papers (or paths) of different roughness on the surface of the sample to be polished. In the laboratory we have paths with different thicknesses and colors, we have the 30mm (green), 15mm (red), 6mm (pink), 3mm (light pink) and 1mm (white).

The following sequence has been followed when polishing:

$$\begin{aligned} 8 \text{ min} &\rightarrow 30\ \mu m \text{ (5 lines)} \\ 8 \text{ min} &\rightarrow 15\ \mu m \text{ (4.5 lines)} \\ 10 \text{ min} &\rightarrow 6\ \mu m \text{ (2.5 lines)} \end{aligned}$$

11 min → 3 μm (Almost 2 lines)
7 min → 3 μm (not even 1 lines)
5 min → 1 μm (not even 1 lines)

As we can see, we start with the ones that have a higher roughness. This is done because these are the ones that wear the material faster. At first, you start with a material with many inequalities, when polishing with the 30 μm path, the material wears out and you get a uniform roughness in it, although not the desired one, because the material still has some roughness because the path is not very fine. A progressive descent is made because perhaps the 1μm path would take hours to polish all the roughness that the 30 μm path leaves us, since this one wears the material very slowly.

3.3.9 Chemical attack on the diffraction grating

It is known that when a crystal structure has suffered a distortion of its crystal lattice, it is much easier to dissolve this part of the crystal. The crystal in its original state is attacked a few nanometers in hours, however when it is subjected to the stress produced by the laser, we see that this changes, attacking a few micrometers per hour. During the attack it is necessary that the particles generated inside the pores by the reaction, such as aluminum, are expelled from the pore in order for the attack to continue moving inward. Therefore, what we achieve during the attack is to empty the pores that we have previously engraved, leaving air ducts inside our crystal and obtaining our diffraction grating.

In these two fabrications we have carried out two types of attacks. The one that we will call standard attack, since it is the one that has always been performed in the laboratory, and then another type of attack. The only thing that changes between the two attacks is the type of dissolution and the method used to clean the pores.

The process to enhance an attack is very simple. First we put the sample in the oven at a temperature of 100ºC, so that the material will expand and the pores will become smaller. When the crystal is already hot, we put it immediately in the solution, so that the crystal cools inside the mixture, expanding its pores and producing that more amount of attack solution enters inside the pores. And with that, we would already have the crystal attacking.

For the standard attack the solution in which we will put the mixture will be of:

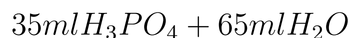

$$35ml H_3PO_4 + 65ml H_2O$$

One of the possible reactions that will occur within the pores is given in [7] and has the following form:

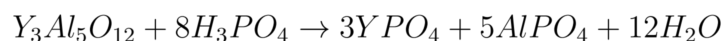

$$Y_3Al_5O_{12} + 8H_3PO_4 \rightarrow 3YPO_4 + 5AlPO_4 + 12H_2O$$

We will put this solution on a heating plate with a magnetic stirrer. By heating the mixture

we are going to make it less viscous so that it can go deeper into the pores and the magnetic stirrer is used to constantly move the solution so that all the remains produced by the attack inside the pores come out.

For the second type of attack, the following mixture was used:

$$30mlH_2SO_4 + 30mlH_3PO_4 + 60mlH_2O$$

And this time the mixture will not be heated as we will use an ultrasonic bath to remove the attack remains from the pores.

3.4 Manufacturing

3.4.1 Work results

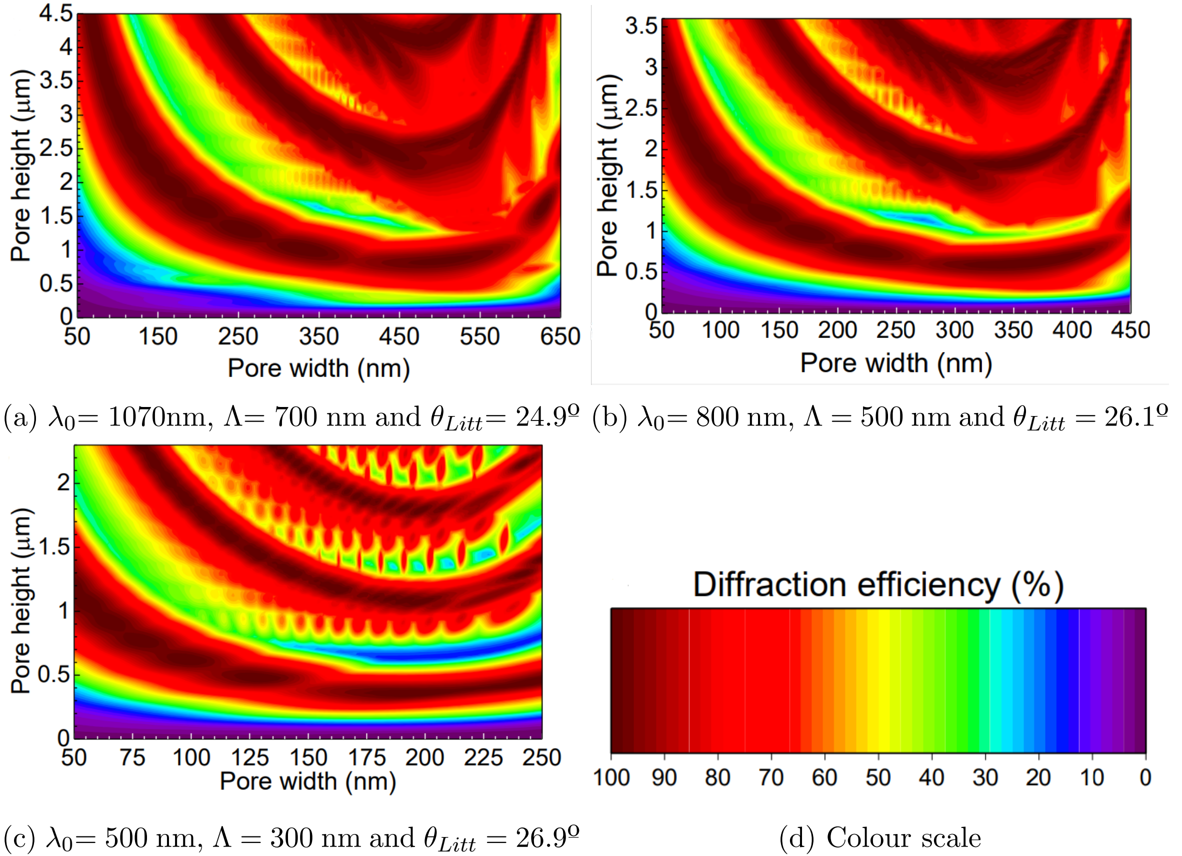

(a) λ_0= 1070nm, Λ= 700 nm and θ_{Litt}= 24.9º (b) λ_0= 800 nm, $\Lambda = 500$ nm and $\theta_{Litt} = 26.1$º

(c) λ_0= 500 nm, $\Lambda = 300$ nm and $\theta_{Litt} = 26.9$º (d) Colour scale

Figure 18: Colourmaps of optimized pore sizes, in which its diffraction efficiency (at first order in transmission) is maximum

In Figure 18 we can see the results obtained in some simulations performed in [1]. We are looking for our grating to have a very high diffraction efficiency, i.e., that almost all the initial intensity of our laser (which is a monochromatic beam) is diffracted in the first diffraction order. That is, to make that a diffraction grating has the maximum efficiency, it is not enough only to diffract the light in the angle θ_{litt} but also, depending on the length and width of the written pore, the gratings will have different efficiencies in transmitting light.

We specifically want to try to make a very high efficiency diffraction grating with a lattice period of Λ= 500, so we are only interested in the Figure 18b. This simulation, as shown in the caption, is optimized for a laser with λ_0 =800 nm and an angle of θ_{litt} = 26.1º. We are going to take a range of height and width and, from there, we will select different points that are in or close to a zone of maximum efficiency. We will cover a range of pore widths from 150 nm to 350 nm and for the heights we will go from 500 nm to 1200 nm.

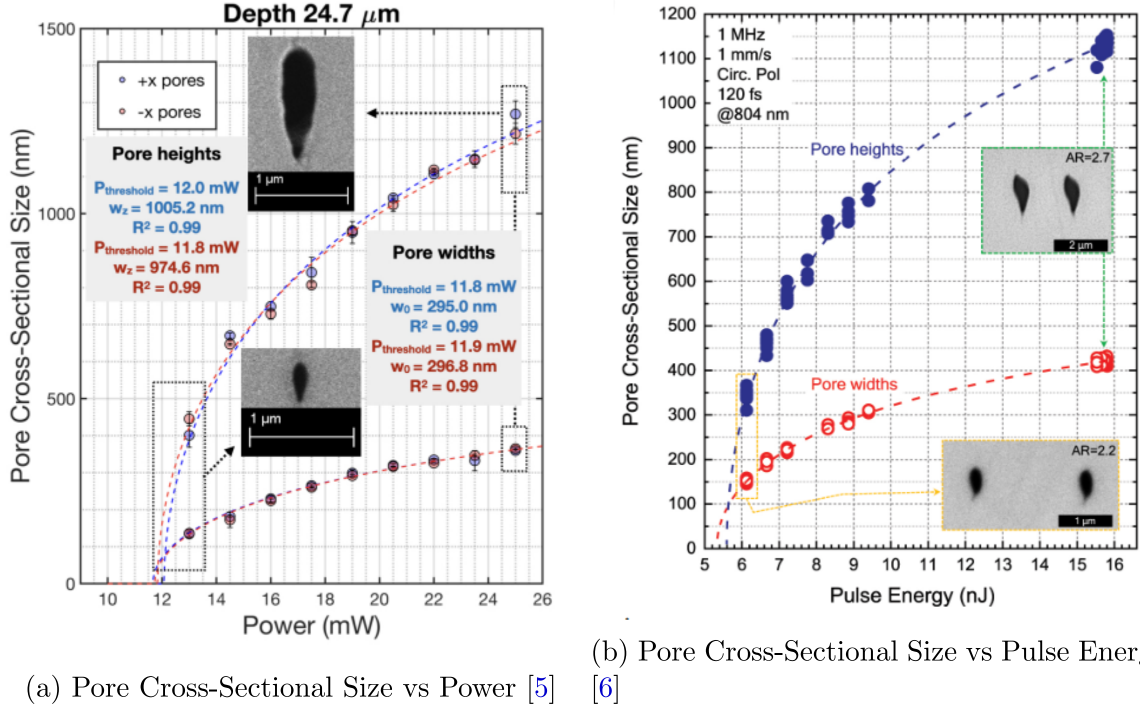

(a) Pore Cross-Sectional Size vs Power [5]

(b) Pore Cross-Sectional Size vs Pulse Energy [6]

Figure 19: Pore size as a function of power/energy of the pulse

For the Figure 19a we can see different pore sizes depending on the power selected. We can see that for this graph, the range that corresponds to the previously selected invervals is from 13 mW to 23.5 mW in width and from 13.5 mW to 25 mW in height. We can see that the ranges in width and height do not cover the same powers but they are close, which is very beneficial to make our diffraction grating.

For the second of the graphs 19b we see that the intervals change. We have a write speed of 1 $\frac{mm}{s}$ and a repetition rate of 1MHz. This graph is plotted as a function of pulse energies, unlike the previous image. As we in the laboratory can only control the power, we will calculate the powers. The formula that relates the pulse energy in nJ with the power in mW is given in 6 where f is the repetition rate.

$$P(mW) = \frac{Ep(nJ)}{10^6} \cdot (f(KHz) \cdot 1000) \tag{6}$$

Substituting, we obtain that Ep (nJ) = P (mW). Then, for this figure, the optimum ranges selected go from 6 to 11 mW for the width and from 7 to 16 for the height. We can see that the difference between both ranges is quite remarkable, since for the pore height we have 10

powers in that interval and for the width we only have 6.

Finally, it has been concluded that the gratings will be manufactured using powers ranging from 10 to 22 mW.

3.4.2 First manufacture

For the first of the fabrications we have used a fragment of a YAG crystal that had already been used by my colleagues who are doing another TFG with the same tutor. For this reason, in some images we can see structures that do not correspond to that of a diffraction grating.

To operate the laser we use a code, which can be seen in its entirety in Annex 1, in this section I will limit to explain what the code does.

The objective to make a diffraction grating is to engrave horizontal lines all over the crystal, although we cannot start engraving from the end of the crystal because it would form cracks, so we always start engraving a little more to the center. This is the reason why we have to polish the sides of the sample, because when you start a little more to the center the pores are covered by the crystal, and to attack them, it is crucial that the pores are exposed. In this fabrication we are going to engrave lattices with five different powers, these will be 22 mW, 19 mW, 16 mW, 13 mW and 10 mW. The lines that we will engrave in the grating will have a length of 4.47 mm, and we will engrave 3200 lines for the same power, separating 0.0005 mm between them (this will be the grating constant Λ), therefore, we will have diffraction gratings of 1.6 mm. The engraving speed has been 10 $\frac{mm}{s}$ and overscan has been performed. The overscan consists of first engraving from right to left and then passing through the same line in the opposite direction.

The depth at which the grating was engraved was 0.025mm from the surface.

As will be seen in the following sections, there have been problems when engraving the grating, because, as the pores have been attacked, only certain regions of what would be the diffraction grating can be appreciated. This has happened because while the diffraction grating was engraved, the temperature of the laboratory has been varying, causing the focus to vary and therefore the grating is not well engraved.

Actually, the lines in the diffraction grating are not engraved as a line, rather it is composed of many dots that form a line. These dots are generated by femtosecond pulses which will have a certain amount of energy depending on the power at which we are engraving. For the fabrications, a repetition rate of 1 MHz was configured, i.e. 1 million pulses are emitted per second.

Now, we are going to calculate the energy of each pulse as a function of its power. To do this, we will start from the equation 6

Isolating Ep we obtain the equation that will allow us to calculate the energy of each pulse as

a function of frequency:

$$Ep(nJ) = \frac{P(mW) \cdot 10^3}{f(KHz)} \tag{7}$$

As the f in this case is 1000 kHz we obtain that Ep (nJ) = P (mW).

In order to be able to make a later study of the chemical wet etch rates as a function of pulse energies and to be able to compare them satisfactorily, it is important to calculate the **pulse dose** in the material.

The pulse dose in a material is the number of pulses per meter that a sample has. To easily calculate the dose, we will start by calculating the pore spacing. To do this we will use the equation 8

$$Pulseseparation(\frac{mm}{pulse}) = \frac{SPEED(mm/s)}{f(kHz) \cdot 1000} \tag{8}$$

For our case, the speed was 10 $\frac{mm}{s}$ and the repetition rate was 1000 kHz, obtaining that it is 0.00001 $\frac{mm}{pulse}$, and therefore we will have a separation between pulses of 10 nm. If, for example, we consider that the spot size is 600 nm this gives us that we have an overlap of 6 pulses.

Once the pulse spacing is known, it is easy to calculate the number of pulses in 1 meter. Making a simple rule of three, we obtain that the pore dose is $10^8 \frac{pulses}{m}$. Since overscan has been performed in this case, we will say that the dose is overwritten.

3.4.3 Second manufacture

For this second production we decided to change some things with respect to the first. This time, instead of 5 powers, we will engrave using 6 powers, these were 22 mW, 20 mW, 18 mW, 16 mW, 14 mW and 12 mW. As the crystal this time was 9.8 mm long and 4.9 mm wide, we changed the length of the engraved lines to 4.7 mm. The distance between lines and the length of the diffraction grating were the same as in the previous fabrication, 0.0005 mm and 1.6 mm, for each power. This time no overscan was performed, so one line was recorded in one direction and the next one in the opposite direction. It is important to note that while the lattice was engraved, two lines were made in a row without closing the shutter, leaving between the two lines another line joining their right ends. This may result in an increase of cracks at the ends, but as they have to be polished afterwards, this was underestimated. The scanning speed for this fabrication has been 1 $\frac{mm}{s}$ unlike the previous fabrication which was 10. In this case, we left a space of 0.04 mm between each power, so that it is much easier to distinguish them.

For this case, the repetition rate was also 1000 KHz. We can say according to the equation 7 that, as in the first fabrication, the Ep (nJ) = P (mW). That is, the power will be equivalent to the energy of each pulse.

The separation between pulses will be different from the one for the first fabrication, since in

this case the speed will be 1 $\frac{mm}{s}$. Therefore, substituting in the expression 8, we obtain that the separation between pulses is 0.000001 mm, i.e. 1 nm. Making a rule of three, we obtain that the number of pulses in one meter, that is, the dose for this fabrication, is $10^9 \frac{pulses}{m}$.

The dose can also be set as a function of the pulse energies, this is done by multiplying the dose value obtained by the pulse energy of each power. This gives us that the pulse energies are $22 \cdot 10^9 \frac{nJ}{m}$, $20 \cdot 10^9 \frac{nJ}{m}$, $18 \cdot 10^9 \frac{nJ}{m}$, $16 \cdot 10^9 \frac{nJ}{m}$, $14 \cdot 10^9 \frac{nJ}{m}$ and $12 \cdot 10^9 \frac{nJ}{m}$.

3.4.4 Diffraction angle measurement experiment

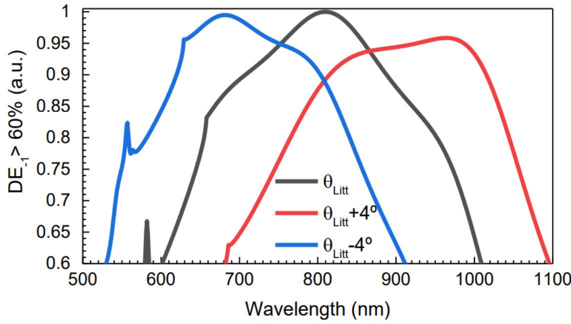

Figure 20: Diffraction efficiency according to wavelength and angle used [1]

We know that the optimizations made in Figure 18b are designed for a laser with a $\lambda_0 = 800$ nm but our laser has a wavelength of $\lambda_0 = 1070$ nm (for the first harmonic). Therefore, for our laser we could achieve a theoretical diffraction of 91% (approximately) if we exceed the Littow angle by 4º more.

4 Analysis and discussion of results

En esta sección se van a discutir los resultados obtenidos en la fabricación de las redes de difracción. En primer lugar, discutiremos como han ido aumentando las longitudes de los nanoporos a medida que atacábamos la muestra en nuestra primera fabricación. Como veremos la primera fabricación no salió muy bien, pues no se grabaron todas las potencias y con el paso de los ataques se ve la red de difracción muy dañada a causa de los craks, esto no nos permitirá extraer resultados fiables. Después de la discusión de la primera fabricación pasaremos a hablar sobre como han ido evolucionando las longitudes de los nanoporos para la segunda. Concluiremos que las energías de pulso más intensas empiezan atacándose más rápido, pero decae su ritmo de ataque con más velocidad. A diferencia de las potencias menores, las cuales empiezan atacándose más lento, pero en los ataques finales son las que tienen mayores ritmos de ataque. También estudiaremos lo que pasa dentro de los nanoporos durante el ataque ajustando nuestros resultados a una función de difusión 5 y analizando los coeficientes que obtenemos para cada una de las potencias.

As mentioned in the methodology, two diffraction gratings have been performed on YAG crystals with the first harmonic of the laser we have in our laboratory.

4.1 First manufacture

4.1.1 Observation under the optical microscope before starting to attack

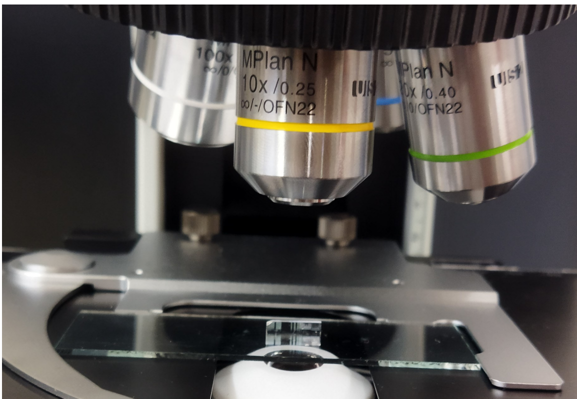

Figure 21: Position of the sample to observe the pores

Before starting we must wash the crystal with acetone, that is done to be able to see more clearly the sample. In the Figure 22 we can observe the images taken in the microscope, for it has been placed the sample as it is appreciated in the Figure 21. As is known, the pores of our grating are lines separated by 0.0005 mm, so at 10x magnification only a long line will be visible. In some images we can see the structures made by a colleague [5] which are seen as 4 points in a row. Using the different filters in our laboratory optical microscope, we can observe how the optical properties of the crystal have changed as our diffraction grating was engraved.

In Figure 22a we can see our sample without any filter, this type of image is called Koehler and is made by putting the microscope in transmission, the numerical aperture equaling that of the objective and the shutter open to the maximum.

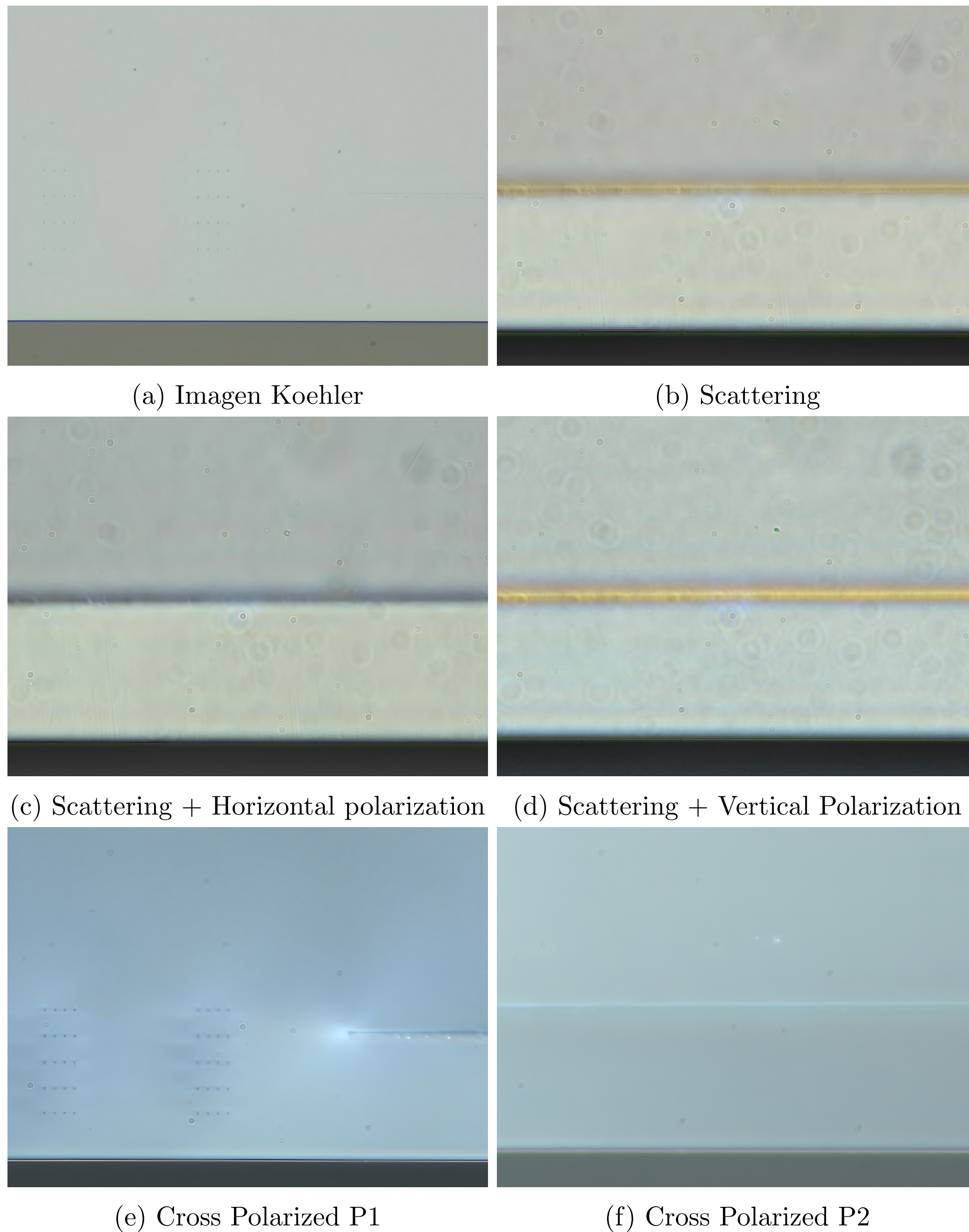

(a) Imagen Koehler (b) Scattering

(c) Scattering + Horizontal polarization (d) Scattering + Vertical Polarization

(e) Cross Polarized P1 (f) Cross Polarized P2

Figure 22: Images of the first manufactured volume diffraction grating

In the Figures 22b, 22c and 22d we can appreciate the scattering of our diffraction grating. In the Figure 22c we can see that if we polarize the light horizontally the guide appears black indicating that it does not guide light horizontally. On the other hand, we can see in the Figure 22d that it does guide vertically polarized light, since the grating is illuminated orange. This means that the diffraction grating on the crystal has produced an anisotropic index change, i.e., it transmits light in one direction but not in the other. In Figure 22b we see how the scattering is seen in the diffraction grating without any polarization, as in these appear the two directions of polarization together, we see that it guides light but not as much as in the vertical polarization.

In the Figures 22e and 22f we can see the sample in cross polarization, in this one the microscope is still in transmission although 2 filters have been put in between, one of horizontal polarization and one of vertical polarization. This type of image allows us to see the areas of the crystal with stress, being shown more illuminated than the rest. In Figure 22e we can see that in the beginning of our diffraction grating the crystal is under more stress than in the rest of the grating. In Figure 22f we can see that the lattice is under more stress than the rest of the crystal, i.e., when the laser is engraved on the crystal, the stress on the crystal increases and thus the risk of nanocracks.

4.1.2 First Etch

For this first etch, we wanted to test the new attack mentioned in the section 3.3.9

The first attack lasted 174 minutes, approximately three hours. We can see in the Figures 23a, 23b and 23c that the pores have been attacked very little, so the new attack method used must not be very efficient, so we are going to perform the attacks as usual. We can see in Figure 23a that many nanocracks have been produced, especially for the 22 mW power (the most intense).

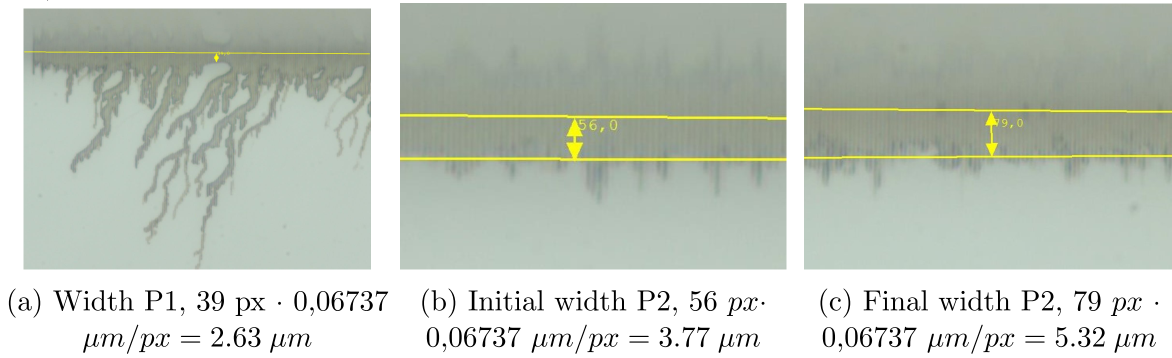

(a) Width P1, 39 px · 0,06737 $\mu m/px = 2.63\ \mu m$ (b) Initial width P2, 56 $px \cdot$ 0,06737 $\mu m/px = 3.77\ \mu m$ (c) Final width P2, 79 $px \cdot$ 0,06737 $\mu m/px = 5.32\ \mu m$

Figure 23: Microscope measurements of powers 1 and 2. Images taken with the 100x objective.

4.1.3 Second Etch

For the second etch, the standard attack was used, as it has been found to be more effective.

In Figure 24 we can observe four images of the first two powers taken with the microscope at 10x magnification. In the first three, we see the pore length of the first power, i.e. the one with a pulse energy of 22 nJ and in the last one we see the second power of 19 nJ. If we look closely at the figures 24a and 24b we can easily distinguish 2 attacked zones, one darker than the other. The darker area is a region where cracks have been produced, preventing the correct functioning of the diffraction grating, since light will not be transmitted through this region as a diffraction grating would. This can be seen in the images shown in later attacks.

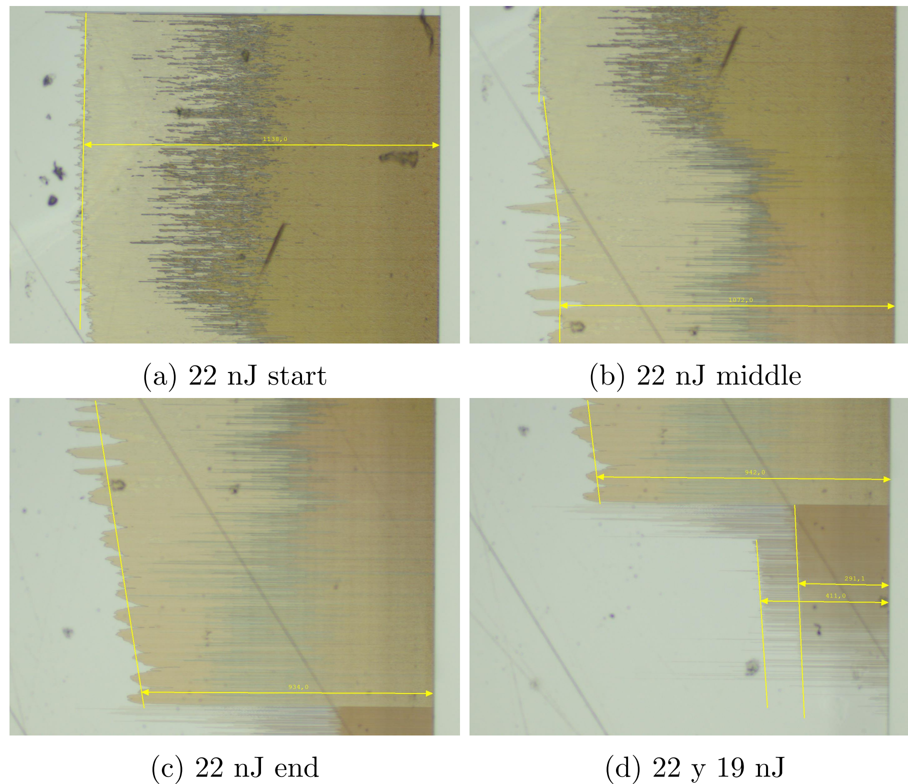

(a) 22 nJ start (b) 22 nJ middle

(c) 22 nJ end (d) 22 y 19 nJ

Figure 24: Microscope measurements of the pulse energies of 22 and 19 nJ. Images taken with the 10x objective..

The lengths obtained for the 2 powers shown in the images were 716.72 for the first (22 nJ) and 281.08 for the second (19 nJ).

4.1.4 Third Etch

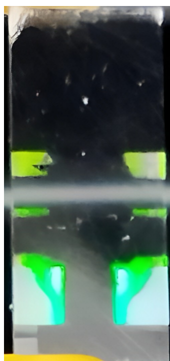

Figure 25: Third Etch

For the third etch the standard etch was used again. The measurements of the first 2 powers were taken with the help of the microscope, and with the Image J [8] program we measured the length of the nanopores of the third power.

As mentioned before, the whole grid was not engraved, this is clearly seen in the Figure 25 where only three fragments can be seen. In the bottom fragment we find the 22 mW power together with a very small segment of the 19 mW power. The middle fragment corresponds to the 19 mW power and the last one is part of the 16 mW power. In the first of the power we see that there is a white region, these are cracks that do not let the light transmit correctly.

To see the cracks more clearly we can look at Figure 26 which shows an image of the first power under the microscope at 10x magnification.

Figure 26: Cracks energía 22nJ

It can be seen in the figure on the right two areas, as discussed in previous sections, the first area corresponds to the darker region and the second to the lighter region. The first region is formed by

internal cracks produced by the stress of the material, in this region the light is transmitted in the way it wants because the cracks have damaged the entire structure that we have recorded. In the second region we find pores without cracks, that is why in this area we can see the transmission of our diffraction grating.

If we pay special attention to the two images we can associate the fragment shown in Figure 26 as the part where the cracks of the first power start to reduce their size. As can be seen the cracks look white because they do not transmit the light in the way they should.

The measures obtained by measuring the different lengths in this attack, which lasted 69 h, were 1351.37 μm for the 22 nJ power, 1015.58 μm for the 19 nJ power and 960.41 μm for the 16 nJ power. We see how the first of the powers is being attacked the fastest.

4.1.5 Fourth Etch

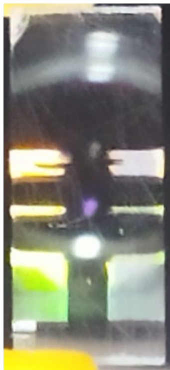

Figure 27: Fourth Etch

This was also a standard attack and lasted approximately 100h.

In Figure 27 we can see how our diffraction grating looks like once the sample of the fourth attack has been removed. Although in this image the cracks are not as noticeable as in Figure 25 the cracks are still there, but due to the illumination it may seem that there are not any more.

In this attack, a pore length of 1534.78 μm has been obtained for the 22 nJ pulse energy, 1419.73 μm for 19 nJ and 1480.52 μm for 16 nJ. We now see that the third power has surpassed the second power.

4.1.6 Fifth Etch

The fifth etch was the last to be carried out, this was a standard attack and lasted 97h. Counting the hours of attack we get a total of 290h.

In Figure 28 we can appreciate how the crystal has looked like once all the attacks have been carried out. To begin with, we can see that at the 22 mW power, the two ends of the crystal have been joined, leaving the entire diffraction grating attacked. Although it has been attacked completely, we can also see that, in a large part of the network, the cracks have been attacked, preventing the proper functioning of the lattice in that area. We can see that the crack line of the first power has been leveled, i.e., the length of the cracks is approximately the same throughout the power, unlike what we could appreciate in Figure 25. The 19 nJ and 16 nJ pulse energies, although they have not attacked the nanotracks completely, we can see that they have no cracks.

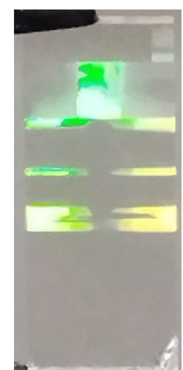

Figure 28: Fifth Etch

The pore distances finally obtained were 2036.22 μm for the 22 mW power, 1699.02 μm for the 19 mW power and 1773.52 μm W for the 16 mW power.

4.2 Second manufacture

4.2.1 First Etch

In this first attack a standard attack has been made. The mixture used had already been used in previous attacks, so the proportions are probably different from those mentioned in 3.3.9. We have seen that pores of the same power have been attacked disuniformly, so values of these lengths have been taken and plotted (Figure 29).

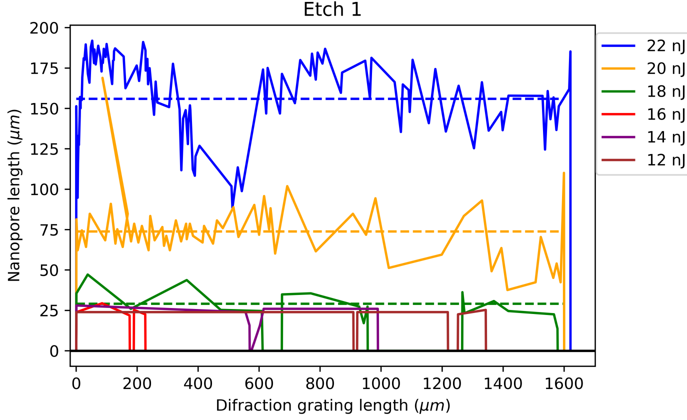

Figure 29: Pore attack length

Figure 30: X and Y axes

As it may be a bit confusing that length vs. length has been represented, in Figure 30 it is shown which are the x and y axes represented in Figure 29. We can see, in Figure 29, that the powers that have been attacked more disuniformly are 22 mW and 20 mW, i.e., the most intense powers have been attacked with more irregularity. The 18 mW and 16 mW powers have irregularities but not as many as the first two. On the other hand, in the last two powers (14 mW and 12 mW) the pores have been attacked almost uniformly. Perhaps these irregularities are related to the greater presence of cracks in the first two powers, these cracks have been generated because the stress to which the crystal is subjected is greater as the power is higher.

In order to know the average lengths of the nanopores, the average was made excluding those points where the distance was 0. These averages are represented in the first 3 powers by dashed lines in Figure 29. The averages of the different attacks have been for the 22 nJ pulse energy 155.98 μm, for the 20 nJ 73.94 μm, for the 18 nJ 29.17 μm, for the 16 nJ 24.62 μm, for the 14 nJ 22.56 μm and for the 12 nJ 23.93 μm. We can see that in this first attack the higher the power the longer the nanopore has been, except for the last power which has surpassed the 14 mW one.

4.2.2 Second Etch

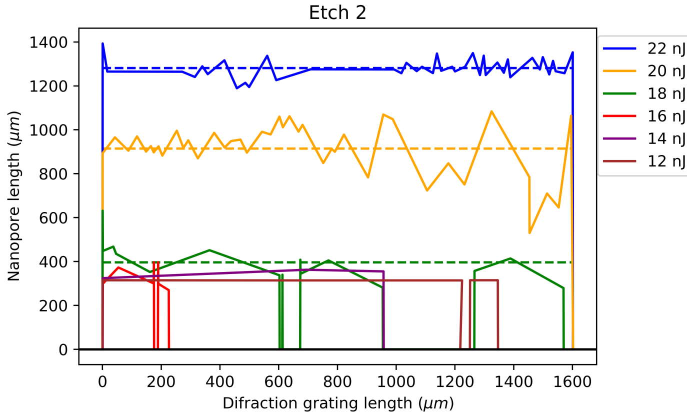

Figure 31: Pore attack length

For the second attack, the solution used in the first attack was reused; by reusing it so many times, the amount of water is reduced, deviating us from the optimal point of attack. The pores continued to attack in a non-uniform way, as can be seen in the Figure 31, especially those of the two highest powers. The attack lasted a total of 97 h.

The average lengths achieved by the nanopores for this second attack were 1281.32 μm for the 22 nJ, 914.68 μm for the 20 nJ, 396.70 μm for the 18 nJ, 333.25 μm for the 16 nJ, 347.19 μm for the 14 nJ, and 314.32 μm for the 12 nJ.

4.2.3 Third Etch

For the third attack we added attack solution to the mixture that was being used for attacking. Therefore, the acid used for etching was diluted, making the mixture less viscous, even though the mixture was not at the optimum etching point.

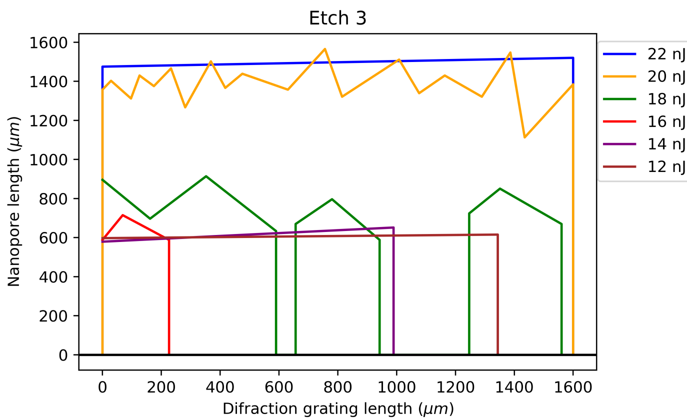

Figure 32: Pore attack length

This attack lasted 68 h and in Figure 32 we can see the attack lengths of the different pores. This time the microscope was not used to measure the attack length, since the attack distance was much larger than the microscope aperture, making it difficult to take data. To measure it more easily, the sample was photographed (Figure 33) and then the Image J application [8] was used to calculate the distance of the pores.

Figure 33: Third Etch

We can see that in both figures 32 and 33 the first power (22 nJ) has reached a uniformity in the pore attack length, that perhaps means that this is the attack limit of the first power and that going beyond that is going to be quite difficult. In the second power we continue to find inequalities in the attack length, and the other powers continue with fairly uniform lengths.

The attack lengths acquired in this attack number three (subtracting the distance of this attack minus those of the previous one) have been 216.50 μm for the first pulse energy (22 nJ), 475.87 μm for the second (20 nJ), 347.24 μm for the third

(18 nJ), 297.24 μm for the fourth (16 nJ), 268.23 μm for the fifth (14 nJ) and 292.07 μm for the sixth (12 nJ). We can see that the first power has the shortest attack length, which again indicates that the 22 mW power is reaching its attack limit as predicted by the fact that the lines of the first power had equalized. The attack lengths of the other powers have maintained the same trend as in the previous attack, with the exception of the 12 mW power whose attack length is longer than the 14 mW power.

The etch lengths shown in Figure 32 are the total lengths, i.e. adding the distances acquired in the different attacks. It is for that reason that the first power still has a greater attack length, since if we add the three attacks we are left with a distance of 1497.82 μm. The other powers have a total length of 1390.55 μm the second (20 nJ), 743.94 μm the third (18 nJ), 630.49 μm the fourth (16 nJ), 615.42 μm the fifth (14 nJ) and 606.38 μm the sixth (12 nJ). We see that the powers continue to have greater length at higher power.

4.2.4 Fourth Etch

In the fourth etching we continued to use the same solution as in the third etching. This attack lasted 288 h, therefore the crystal has been under attack for 455 h.

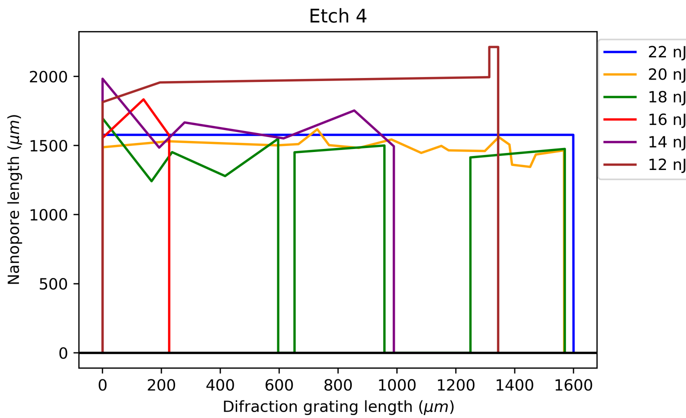

Figure 34: Pore attack lenght

In Figure 34 we can see the total final attack length for each of the different powers. These distances will be 1577.02 μm for the first pulse energy (22 nJ), 1484.27 μm for the second (20 nJ), 1450.84 μm for the third (18 nJ), 1654.36 μm for the fourth (16 nJ), 1655.58 μm for the fifth (14 nJ) and 2037.99 μm for the sixth (12 nJ). We can see that power 6 is the one that has reached the longest attack length, with the two ends of the lattice coming together in the last nanometers of the power. The other powers have reached more or less the same nanopore length.

Considering only the nanopore lengths acquired by this attack we obtain 79.19 μm for the first (22 nJ), 93.72 μm for the second (20 nJ), 706.90 μm for the third (18 nJ), 1023.88 μm for the fourth (16 nJ), 1040.16 μm for the fifth (14 nJ) and 1431.61 μm for the sixth (12 nJ). We can see that now the lowest powers have been attacked the most.

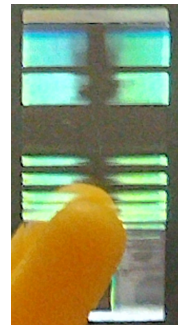

Figure 35: Fourth Etch

In Figure 35 we can see how our diffraction grating looks like once the attacks are finished. We can see that the first two powers (the ones under the tweezers) do not diffract the light very well, this is due to the fact that when these powers were engraved the damage in the form of cracks on the crystal was very high, so

the cracks have been attacked and the diffraction properties of the lattice have been damaged. For the other powers we see that the attack has been very effective, because thanks to this last attack the distance of the nanopores of the first power has been reached and even exceeded. We can tell that the crystal has been subjected to attack for many hours just by the way its surfaces are, as these are extremely rough due to some crack formed on the surface.

4.2.5 Sample profile images

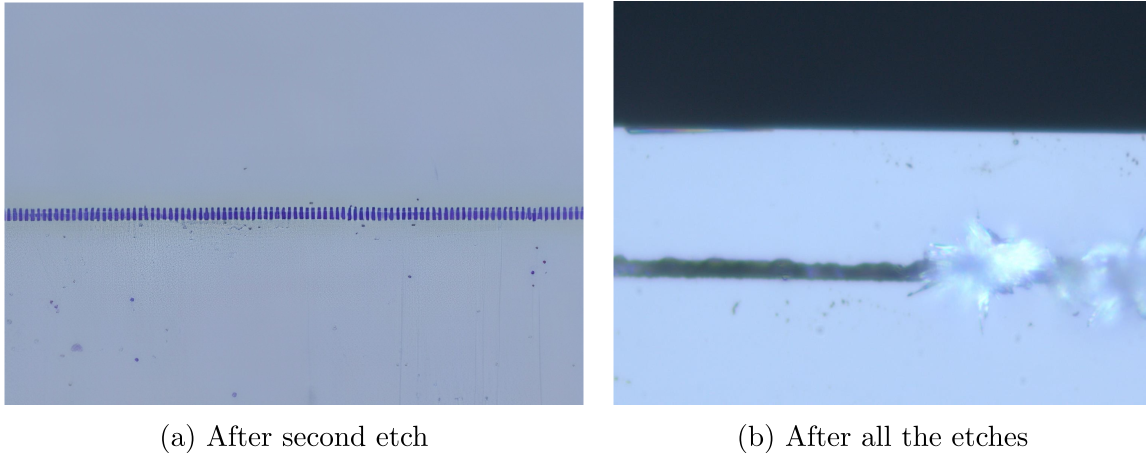

(a) After second etch (b) After all the etches

Figure 36: Crystal profile after second etch and at the end of all the etches

In Figure 36 we can see the crystal profile after two attacks (36a) and when all the attacks mentioned above have been performed (36b). We can see in Figure 36a that it is possible to distinguish perfectly the pores engraved by the laser, because it is seen as a succession of lines placed one next to the other.

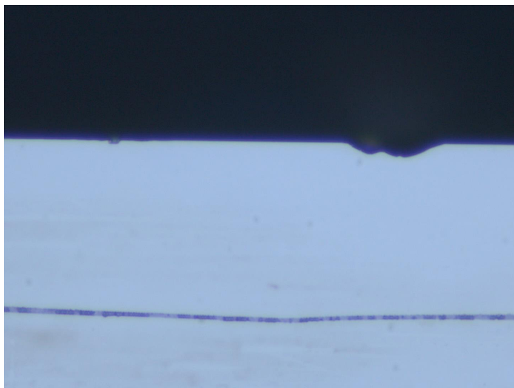

Figure 37: Change of focus during manufacturing

Unlike the Figure 36a, the Figure 36b shows a single line in place of the pores. This single line has probably been generated because during the extensive hours of attack on the sample the edges of the pores have been attacked, becoming larger and joining together. To see the pores again, we should perform another polishing to remove the most damaged outer zone.

In Figure 37 it can be seen how the focus has changed as the diffraction grating has been engraved. As explained above, this is due to the fact that we are not yet able to maintain a stable temperature in the laboratory, causing the focus of the microscope objective to vary as our diffraction grating is recorded.

4.3 Results

We will start the discussion of results by showing the evolution of the irregularities in the nanopore lengths for each of the powers (Figure 38).

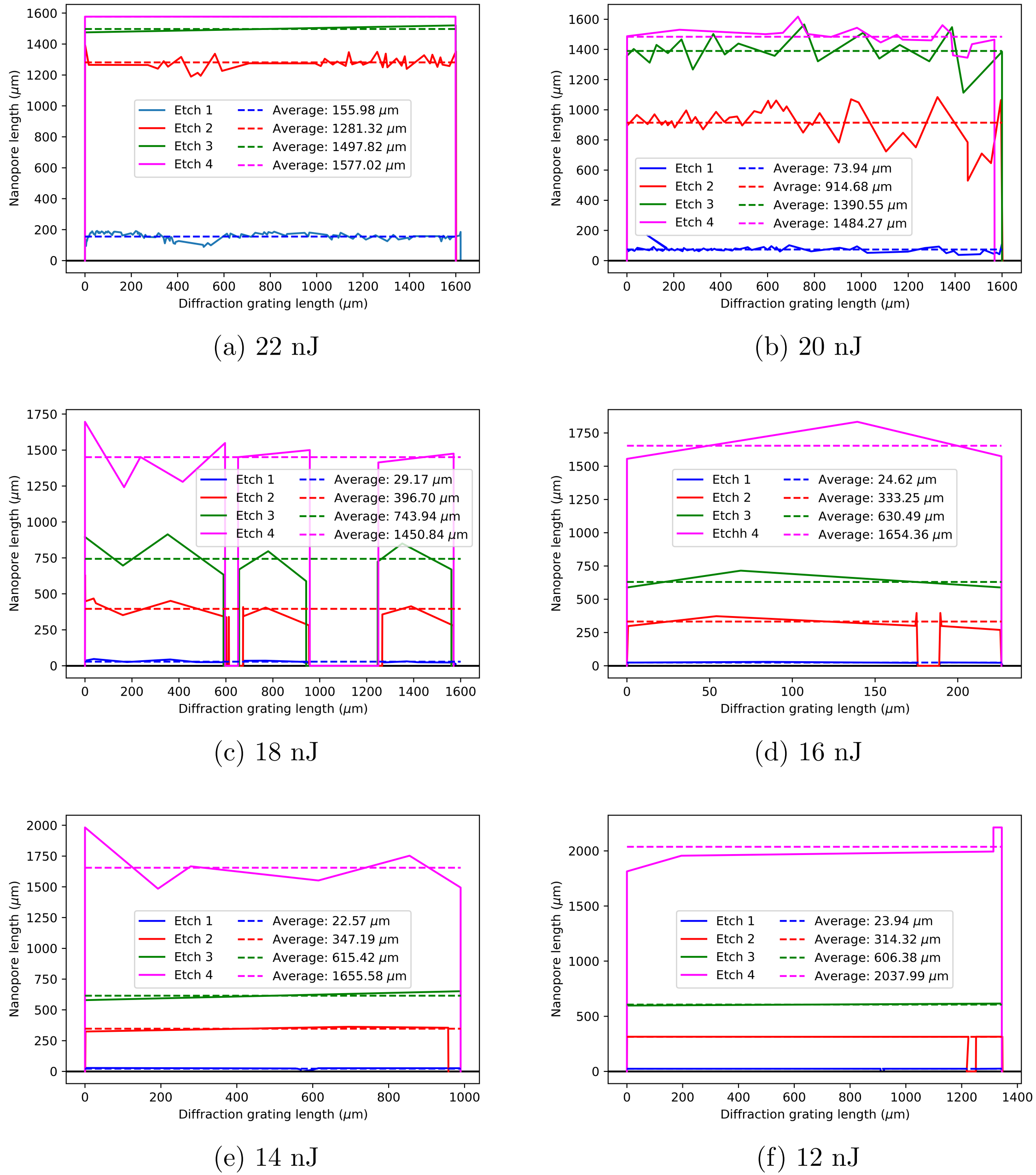

(a) 22 nJ (b) 20 nJ

(c) 18 nJ (d) 16 nJ

(e) 14 nJ (f) 12 nJ

Figure 38: Evolution of the nanopore lengths for the different powers

It is known that the more pulse energy applied to the crystal when poring, the more stress the crystal will have (assuming the same scan speed and repetition rate is used for all) and thus the more nanocracks will be generated. More intense powers start attacking at a higher chemical wet etch rate than lower powers, although they reach modification saturation faster as well. We believe that there comes a point at which the maximum stress that the crystal lattice can withstand is reached and that from then on only internal nanocracks are produced that relax the stress; we will call this point modification saturation. As the higher powers have a higher level of stress, since the modifications in the lattice produced by the laser are greater, they will reach modification saturation earlier. We could say that the first power (22 mW) reaches this

threshold in the third attack, since all the pores are put at the same level and its attack speed decreases a lot. This also happens with the 20 mW power, where we see that the fourth attack has not contributed much to increase the length of the nanopores. That means that the 20 nJ pulse energy reached modification saturation at the fourth etch. For the other powers we see that despite slowing down their chemical wet etch rate, they continue to increase the length of the nanopores without any problem, reaching the point of joining the two parts of the grating for the last of the powers.

If we take the nanpore lengths for each of the attacks and plot them against time we can study how the chemical wet etch rates have evolved for each of the different powers. This is plotted in Figure 39.

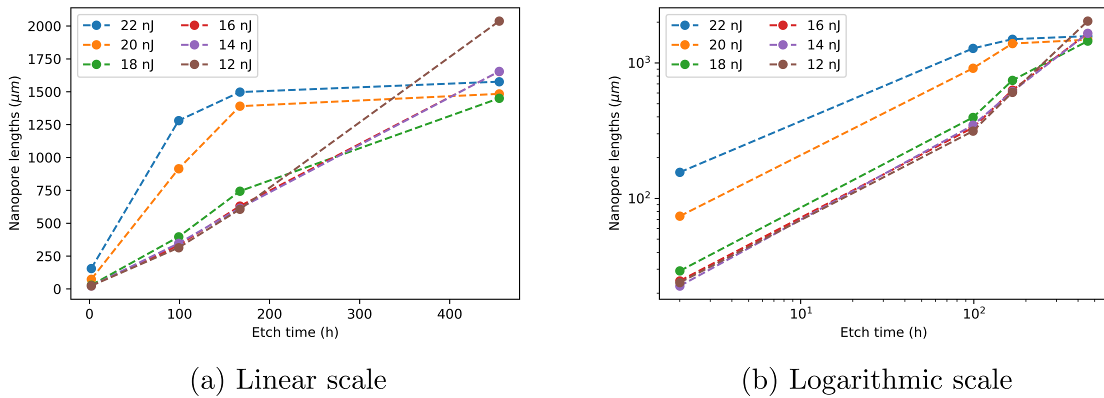

(a) Linear scale (b) Logarithmic scale

Figure 39: Nanopore length vs. etching time

After about 100h of accumulated attack there seems to be a transition in the chemical wet etch rate, decreasing considerably for the two highest pulse energies. Although this only occurs for the first two powers (22 and 20 mW) as in the other cases the chemical wet etch rate seems to increase considerably. This can be seen more clearly in Figure 39b, where the same graph is shown but in logarithmic scale.

We know that once the sample is put under attack there is a diffusion of water and acid into the nanopore, at the nanometer interface between acid and solid, other molecules are generated, and some diffuse out, and some diffuse in. At the nanometer scale this can be considered a chemical diffusion process. If we consider these details we can fit our points to a diffusion function of the type

$$l^2 = 2 \cdot D \cdot t^\alpha \tag{9}$$

Where l indicates the length of the nanopores, D the diffusivity, t the time and α a coefficient indicating the type of diffusivity. In Figure 39, as mentioned before, two zones where the chemical wet etch rate varies can be clearly distinguished, so we will first make a fit to the first two points and then to the last two. Ideally, we would like to measure for many more times and get a much more complete curve of the process. This will allow us to know what is going

on inside the nanopores.

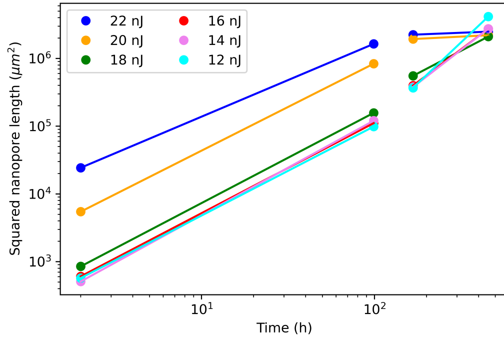

Figure 40: Adjusting to the diffusion function

Once the functions have been adjusted we obtain the coefficients that we were looking for, it has been represented in logarithmic scale since in this way the coefficient α can be known only by looking at the slopes of the straight lines.

In Figure 41 we can see the different α coefficients obtained in the adjustments made.

To begin with, in the first of the fits (first two points) we see for the Figure 41a that the coefficient α is more or less $\alpha = 1.3$ for all powers, this leaves us with a Brownian diffusion tending towards superdiffusive. If we compare the coefficients α with the graph shown in 42 we see that the slopes between the first two points are approximately the same, i.e., the velocity in that interval decays about the same for each of the powers.

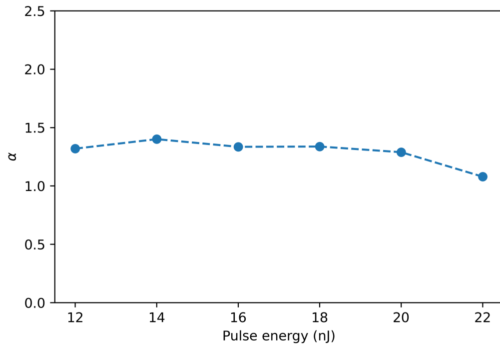

(a) First two points

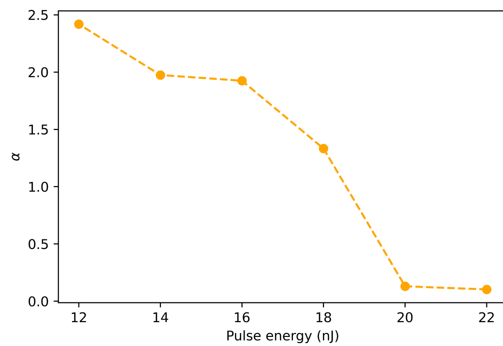

(b) Two last points

Figure 41: Coefficient α vs. pulse energies

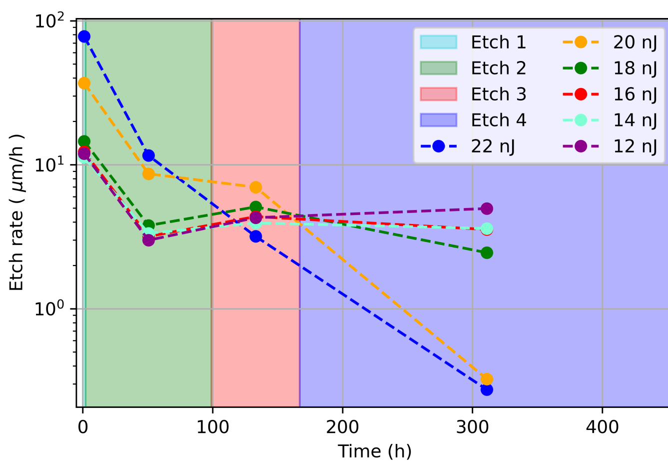

Figure 42: Chemical wet etch rate vs. time

For the second half we see that the coefficients are 2.42 for the 12 nJ pulse energy, 1.97 for the 14 nJ, 1.92 for the 16 nJ, 1.33 for the 18 nJ, 0.13 for the 20 nJ and 0.10 for the 22 nJ. It can be seen, in first place, that the 2 higher powers are facing a subdiffusive diffusion process. This means that the distance traveled by the solution inside the nanopores has been greatly reduced. We believe that by the third etch the

pulse energies of 22 nJ and 20 nJ would have reached modification saturation. This results in what we see in Figure 35, where we see very clearly that in the last attacks only the nanocraks rather than the nanopore lengths have been attacked.

We must think of the crystal lattice as an elastic structure, once the stress is relaxed it returns to its original shape, slowing the rate of attack to what the crystal would have if we had not written the lines. This is what happens when the crystal reaches the modification saturation.

If we now look at the slopes between the last 2 points in Figure 42 and compare them with the coefficients plotted in Figure 41b we can see that they are clearly related. We see that the powers with the steepest slope belong to a subdiffusive diffusion, then we have the 18 nJ pulse energy whose slope is a little less steep than in the previous 2 powers and has a diffusion close to Brownian, lastly we have a superdiffusive diffusion for the 12, 14 and 16 nJ pulse energies, whose slopes are the least steep. In a solution we know that the initial diffusion velocity is much higher than the final one, because as they approach the equilibrium, the concentration gradients are decreasing (because the solution is closer to the equilibrium). Hypothetically speaking the pore velocity should be decreasing over time, but if we look at the lower energies we have a small increase in the velocities between attacks 3 and 4, this can lead us directly to a superdiffusive diffusion, because instead of decreasing, as it should have been, it has increased.

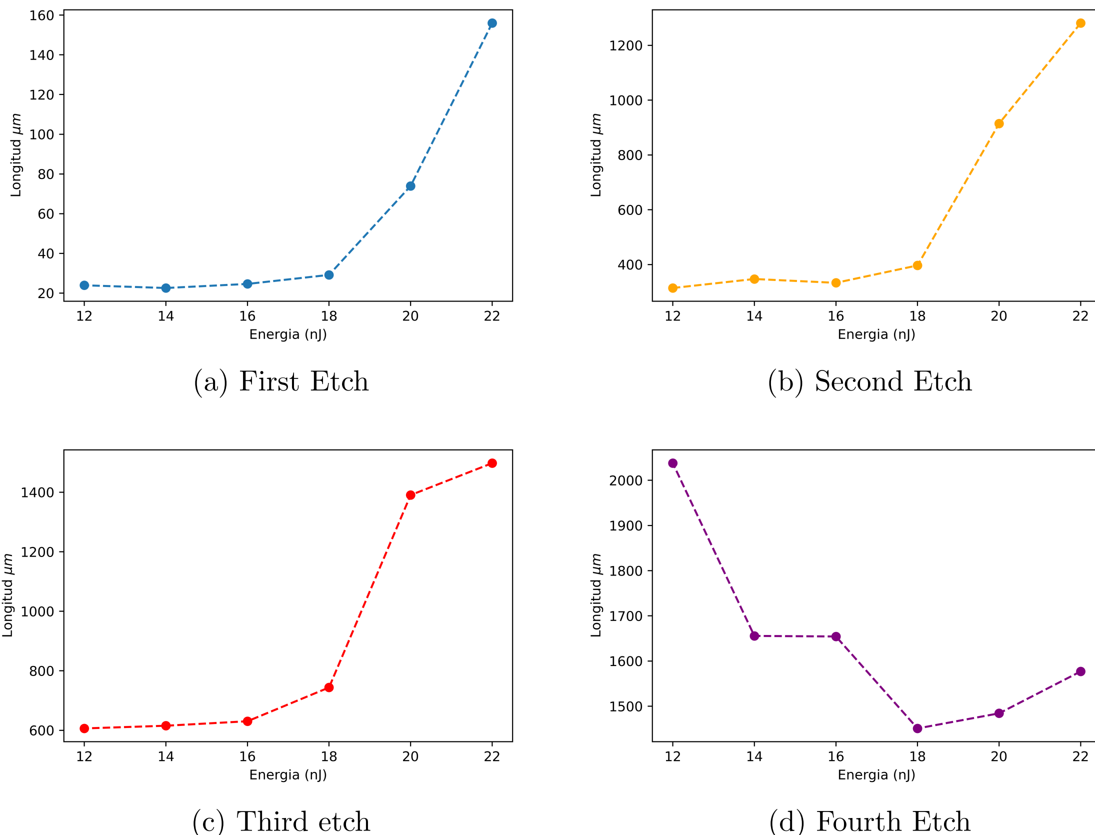

(a) First Etch

(b) Second Etch

(c) Third etch

(d) Fourth Etch

Figure 43: Nanopore length vs. pulse energy

The graphs in Figure 43 show how the nanopore lengths evolved as the attacks progressed. First, if we look at the first two Figures (43a and 43b) we can see that their shape remains more or less constant, this is directly related to the fact that they all have the same coefficient *alpha*. If we now look at figures 43c and 43d we observe that the difference from one to the other graph for the energies of 12 nJ, 14 nJ and 16 nJ has a very similar shape to the one given in Figure **??**, that means the coefficient α is related to the increase in the lengths for each of the attacks.

As results of the first fabrication, a plot of the nanopore lengths versus attack time is shown in Figure 44.

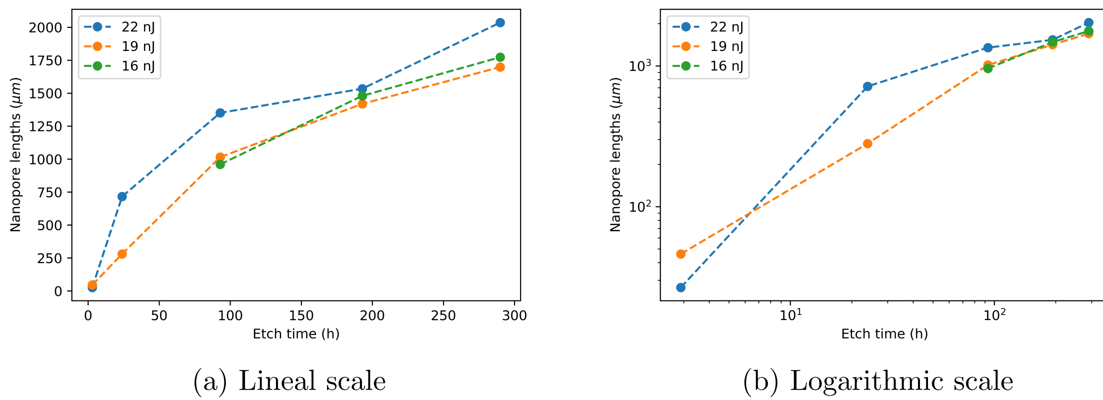

(a) Lineal scale

(b) Logarithmic scale

Figure 44: Nanoporelength vs. etch time (First fabrication)

As expected we see that the chemical wet etch rate is decreasing over time. As could be seen, the first production went a bit wrong, as the entire lattice was not recorded and many craks were generated due to the overscan. For this reason it is not possible to extract quantitative data on the first of the two fabrications.

5 Conclusions and improvement projects

En esta sección se pretende resumir las conclusiones obtenidas, así como explicar algunos proyectos que se quieren realizar en el futuro. Lo primero de lo que se habla es del cambio anisótropo producido al grabar la red, transmitiendo la luz polarizada verticalmente pero no la horizontal. Después se habla de que las potencias más intensas alcanzan más rápido la saturación de modificación, atacándose a partir de ese momento los nanocracks. A continuación se habla de las difusividades obtenidas para cada una de las potencias y se menciona que en un proyecto de futuro se quieren medir más puntos para obtener resultados más concluyentes. En cuarto lugar, se habla de la importancia que tiene controlar la disolución durante los distintos ataques, ya que a medida que se va reutilizando la disolución nos vamos alejando del punto óptimo de ataque. Después se habla de la necesidad de medir los poros y del experimento que se debe realizar en un futuro para medir el ángulo de difracción, permitiéndonos saber si hemos realizado las redes acorde a los estudios realizados en [1]. En último lugar, se habla de una de las maneras en las que se puede lograr que los nanotracks se ataquen por completo, esta consiste en hacer perforaciones que unan el conducto con la superficie a lo largo de la línea grabada, permitiendo atacar los poros desde dentro.

As conclusions it is worth highlighting several things seen throughout the results. First of all, when the diffraction grating is engraved, an anisotropic index is produced, i.e., the diffraction grating will only transmit vertically polarized light and not horizontally polarized light. This is of great interest if we look at the diffraction grating as a wave-guide.

Secondly, we have seen that the powers that are attacked faster at first are those with a higher pulse energy, then these more powerful energies reach modification saturation faster, slowing down their chemical wet etch rate. When this modification saturation is reached, we see that the diffraction grating begins to lose its property of diffracting light, because the ones that are attacked are the internal nanocracks formed during the writing process.

We have seen that depending on the diffusivity obtained we can know what is happening inside the nanopores. In this case, we see that they all start following a Brownian diffusivity and then separate. The 12, 14 and 16 nJ energies become superdiffusive diffusion, the 18 nJ remains constant with Brownian diffusion and the 20 and 22 nJ energies become subdiffusive diffusion. This α coefficient allows us to know how the rate of attack inside the pores varies. In the future we would like to design an experiment to measure more points on the curve of nanopore length versus attack time, so that we could make a fit to the diffusivity function of more than 2 points. Actually with 2 points the results obtained are not very reliable.

As an improvement for the future, I believe that the solutions used for the different attacks should be more controlled. We must think that the solution is only optimized at the beginning, then due to the chemical reaction and the evaporation of the water, the initial optimization is lost. I think that having an optimum solution is essential to be able to compare the

different attacks with each other because if we do not have the same conditions all the time the comparison is not so accurate. For example, perhaps at some point the chemical wet etch rates have decreased because of the dissolution of the attack, and not because they had to decrease.

To see if the powers chosen to make the lattice are adequate, in order to obtain the optimum diffraction gratings we were looking for, it is necessary to measure the width and height of the different pores. As it has been observed in the results section, the edges of our sample were very attacked, not being able to see any pore well. In order to measure the size, it would be of vital importance to polish the outermost area of the edges, so that the nanotracks would be exposed.

In the future it is planned to perform an experiment that measures the diffraction of light, so that the simulations performed in [1] could be corroborated. This was planned to be done in this TFG but due to lack of time it could not be done.

If we want to attack the pores completely, we can make small perforations along the nanotraks that join the surface with the conduit, so that, the dissolution can enter through these openings and can be attacked from the inside.

6 Bibliography

[1] Alfredo Casanovas Melián. Design of sub-wavelength transmission gratings fabricated by means of 3d femtosecond nanolithography, 2020 - 2021.

[2] Universidad de Granada. Sesión 8. redes de difracción. espectroscopia. Link.

[3] Angel Franco García. La ley de snell de la refracción. Link.

[4] Ernesto de Jesús Alcañiz. Difracción. Link.

[5] Marcos Hernández Rodríguez. 2d photonic crystals: Research into the fabrication of 2d photonic structures by means of femtosecond laser nanowriting on laser crystals, 2022-2023.

[6] Airan Ródenas Franzette Paz-Buclatin. Circularly symmetric nanopores in 3d femtosecond laser nanolithography with burst control and the role of energy dose. Nanophotonics, 2022.

[7] Airán Ródenas. Three-dimensional femtosecond laser nanolithography of crystals. Nature Photonics, 2018.

[8] Image J. Link.

7 Annex

7.1 Annex 1: First manufacture code

```
#define ShutterClose $DO0.Z = 0
#define ShutterOpen $DO0.Z = 1

DVAR $FSHIFT $OFSET $DIST $SPEED $SPEEDpos $GratingPeriod $Nlines $GratingWidth
$DEPTH $LDEPTH $ANGLE $PWR $PWR_0 $PWR_Delta $ANGLE_0 $Pmax $Pmin $Pstep
$LossFactor $PWR_Before

' comment
;
// Power Test

enable X Y Z A
ShutterClose

$FSHIFT = 1.3 'Normally is 1.39 for satsuma IFN setup, needs recalibration
$OFSET = 0 'needs calibration

$DIST = 4.47 'total written length of structures (in mm)
$SPEED = 10 'writing speed (in mm/s)
$SPEEDpos = 0.001 'positioning speed
$GratingPeriod = 0.0005 'pore separation (in mm)
$GratingWidth = 1.6
$Nlines = CEIL($GratingWidth/$GratingPeriod) 'number of lines in the grating

$LossFactor = 4.4 'Loss factor of laser power from before the expander to the sample

/////////////'lASER POWER RANGES that reaches the sample///////////
$Pmax = 22 'Maximum desired power mW
$Pmin = 10 'Minimum desired power in mW
$Pstep = -3 'Power step in mW


////////////////////////////////////////////////////////////////////////////////
////////////////////////////////////////////////////////////////////////////////
$DEPTH = 0.025   'depth of structure from the surface (in mm)
```

```
$LDEPTH = ($DEPTH-$OFSET)/$FSHIFT 'Linear movement of the objective such that
the focus is in $DEPTH


////////  PARAMETERS TO CALCULATE THE ANGLE FROM THE DESIRED POWER//////////
////////  TO CALIBRATE THE ANGLE DO FIRST A HARD HOME (HOME BUTTON NEXT TO "A"
  AXIS. ANGLE SHOULD GO TO 0.00º.
////////  THEN MANUALLY INTRODUCE around 47º TO GO CLOSE TO MINIMUM. THEN
  FINE TUNE MINIMUM).

$PWR_0 = 0.5 'Minimum Power in mW
$PWR_Delta = 135-$PWR_0 'Max Power - Min Power in mW
$ANGLE_0 = 41 'Angle shift in degrees (angle where minimum is located)

////////////////////////////////////////////////////////////////////////////////
G92 X0 Y0 Z0 'set surface Z=0 starting point as coordinate origin
DWELL 1

VELOCITY ON 'don't decelerate between moves

Linear Z -$LDEPTH F 1 'goes to starting depth
DWELL 1
////////////////////////////////////////////////////////////////////////////////
ABSOLUTE

FOR $PWR = $Pmax TO $Pmin STEP $Pstep 'repeat every power step

ABSOLUTE
$PWR_Before = $PWR*$LossFactor 'calculate the power needed before the beam expander
CALL GetAngle k($PWR_Before) 'Calculates the corresponding angle for the
 desired power before beam expander
Linear A $ANGLE F 1 'the power is changed to the new given value

REPEAT $Nlines
INCREMENTAL
ShutterOpen
Linear X +$DIST F $SPEED 'writes horizontally (sample moves towards left)
Linear X -$DIST F $SPEED 'writes horizontally (sample moves towards right) overscan
ShutterClose
```

```
Dwell 1

Linear Y +$GratingPeriod F $SPEEDpos 'move to another spot vertically upwards
ENDREPEAT

NEXT $PWR 'ends the power cycling


/////////////////////////////////////////////////////////////////////////////
ShutterClose
END PROGRAM



DFS GetAngle
$ANGLE = ASIN(SQRT(($k - $PWR_0)/$PWR_Delta)) * 180/(2 * Math.PI) + $ANGLE_0
 'PWR must be in mW
ENDDFS
```

7.2 Annex 2: Second manufacture code

```
    #define ShutterClose $DO0.Z = 0
#define ShutterOpen $DO0.Z = 1

DVAR $FSHIFT $OFSET $DIST $SPEED $SPEEDpos $GratingPeriod $Nlines $GratingWidth
$DEPTH $LDEPTH $ANGLE $PWR $PWR_0 $PWR_Delta $ANGLE_0 $Pmax $Pmin $Pstep
$LossFactor $PWR_Before $GratingSpace

' comment
;
// FAB2 GRATINGS TFG NEREIDA VIERNES 28 ABRIL 2023

enable X Y Z A
ShutterClose

$FSHIFT = 1.357 'calibration FAB2 m.hdez.tfg23 - Normally is 1.39 for satsuma
IFN setup, needs recalibration
$OFSET = -0.00139 'calibration FAB2 m.hdez.tfg23

$DIST = 4.8 'total written length of structures (in mm)
$SPEED = 1 'writing speed (in mm/s)
```

```
$SPEEDpos = 0.010 'positioning speed
$GratingPeriod = 0.0005 'pore separation (in mm)
$GratingWidth = 1.6
$GratingSpace = 0.040
$Nlines = CEIL($GratingWidth/$GratingPeriod) 'number of lines in the grating

$LossFactor = 4.4 'Loss factor of laser power from before the expander to the sample

/////////////'lASER POWER RANGES that reaches the sample///////////
$Pmax = 22 'Maximum desired power mW
$Pmin = 12 'Minimum desired power in mW
$Pstep = -2 'Power step in mW


////////////////////////////////////////////////////////////////////////////////
////////////////////////////////////////////////////////////////////////////////

$DEPTH = 0.025   'depth of structure from the surface (in mm)
$LDEPTH = ($DEPTH-$OFSET)/$FSHIFT 'Linear movement of the objective such that
the focus is in $DEPTH


////////  PARAMETERS TO CALCULATE THE ANGLE FROM THE DESIRED POWER//////////
////////  TO CALIBRATE THE ANGLE DO FIRST A HARD HOME (HOME BUTTON NEXT TO "A"
  AXIS. ANGLE SHOULD GO TO 0.00º.
////////  THEN MANUALLY INTRODUCE around 47º TO GO CLOSE TO MINIMUM. THEN FINE
  TUNE MINIMUM).

$PWR_0 = 0.3 'Minimum Power in mW
$PWR_Delta = 525-$PWR_0 'Max Power - Min Power in mW
$ANGLE_0 = 41.15 'Angle shift in degrees (angle where minimum is located)

////////////////////////////////////////////////////////////////////////////////

G92 X0 Y0 Z0 'set surface Z=0 starting point as coordinate origin
DWELL 1

VELOCITY ON 'don't decelerate between moves
```

```
Linear Z -$LDEPTH F 1 'goes to starting depth
DWELL 1
////////////////////////////////////////////////////////////////////////////////
ABSOLUTE

FOR $PWR = $Pmax TO $Pmin STEP $Pstep 'repeat every power step

ABSOLUTE
$PWR_Before = $PWR*$LossFactor 'calculate the power needed before the beam expander
CALL GetAngle k($PWR_Before) 'Calculates the corresponding angle for the desired
 power before beam expander
Linear A $ANGLE F 1 'the power is changed to the new given value

REPEAT $Nlines/2
INCREMENTAL
ShutterOpen
Linear X +$DIST F $SPEED 'writes horizontally (sample moves towards left)
Linear Y +$GratingPeriod F $SPEEDpos 'move to another spot vertically upwards
Linear X -$DIST F $SPEED 'writes horizontally (sample moves towards right)
Linear Y +$GratingPeriod F $SPEEDpos 'move to another spot vertically upwards
ENDREPEAT

ShutterClose
Linear Y +$GratingSpace F 0.1
DWELL 0.1

NEXT $PWR 'ends the power cycling


///////////////////////////////////////////////////////////////////////////////
ShutterClose
END PROGRAM


DFS GetAngle
$ANGLE = ASIN(SQRT(($k - $PWR_0)/$PWR_Delta)) * 180/(2 * Math.PI) + $ANGLE_0
 'PWR must be in mW
ENDDFS
```